[redacted]

JET PROPULSION LABORATORY
CALIFORNIA INSTITUTE OF TECHNOLOGY
PASADENA, CALIFORNIA

RE-ORDER NO.

GER 11156
CODE IDENT NO. 25500

GOODYEAR AEROSPACE
CORPORATION

AKRON 15, OHIO

HIGH-GAIN SPACECRAFT ANTENNA

DESIGN AND DEVELOPMENT

This work was performed for the Jet Propulsion Laboratory, California Institute of Technology, sponsored by the National Aeronautics and Space Administration under Contract NAS 7-100.

GER 11156

Final Report

April 1964

J. W. Haylett

Prepared For

Jet Propulsion Laboratory
California Institute of Technology
Pasadena, California

Purchase Order 950467
(Subcontract under NAS 7-100)

ABSTRACT

20757

Goodyear Aerospace Corporation has concluded a design study resulting in development, fabrication, and delivery of a 9-foot advanced development model of an expandable, directive, high-gain spacecraft antenna for Jet Propulsion Laboratory (JPL). The model demonstrated the feasibility of the design approach resulting from the design study.

This final report documents the program of preliminary design and analysis, model design and fabrication, and model testing; outlines antenna ground deployment procedures; and presents conclusions and recommendations.

Work was done under Contract No. 950467 with JPL. The effort is a subcontract under Prime Contract NAS 7-100.

TABLE OF CONTENTS

LIST OF ILLUSTRATIONS

LIST OF TABLES

SECTION I. INTRODUCTION

A. BACKGROUND

Goodyear Aerospace Corporation has concluded a design study resulting in development, fabrication, and delivery of a 9-foot advanced development model of an expandable, directive, high-gain spacecraft antenna for Jet Propulsion Laboratory (JPL). The model demonstrates the feasibility of the design approach resulting from the design study.

This final report documents the program of preliminary design and analysis, model design and fabrication, and model testing; outlines antenna ground deployment procedures; and presents conclusions and recommendations. Work was done under Contract No. 950467 with Jet Propulsion Laboratory of the California Institute of Technology, Pasadena, California. The effort is a subcontract under Prime Contract NAS 7-100.

The program was initiated by JPL because interplanetary spacecraft antennas considerably larger than current designs are in the forecast of needs for the near future. Due to launch configuration envelope limits considerably lower than the projected requirements, the need for expandable antennas is apparent.

The principal objective of this study was to find practical methods of installing and packaging a 6 to 12 foot diameter aperture on a typical planetary spacecraft. The secondary objective was to provide a design concept that would be practical at diameters in the 25 to 35 foot range. JPL Specifications 15035 and 30257 established design parameters.

The adequacy of design approach was based on reliability and simplicity, weight, state-of-the-art, and radio frequency performance in that order.

B. APPROACH

Design and development approaches were, of course, guided by the performance and product characteristics of the antenna.

The characteristics included the following:

(1) Frequency range of 2295 mc (±5 mc bandwidth) for transmitting and 2115 mc for receiving with ±5 mc bandwidth. Radiated power to be 100 watts c.w. at 2295 mc.

(2) Feed type to be a turnstile one quarter wave over a ground plane 4 inches in diameter.

(3) Nominal reflector shape, f/D = 0.35.

(4) Aperture efficiency not lower than 0.9 db.

(5) Unit aperture weight to fall within the range of 0.3 to 0.5 psf of erected aperture.

(6) Surface tolerance of ± 1/8 inch desired.

(7) Electrical axis alignment shall be adjustable to and maintained at 90(±0.3) degrees to the axis of the support boom at the antenna side of the antenna gimbals. The accuracy is to be maintained in a 0- and 1-g field.

(8) The antenna must be capable of being erected on earth, checked out and aligned, packaged and then re-erected in a space environment, and must always be within specifications.

(9) The antenna shall have a 95 percent probability of erecting sufficiently accurate to fall within the performance required in the specification. Life expectancy after space erection is a minimum of two years.

Goodyear Aerospace first initiated a preliminary design and analysis program to establish guide lines for material selection, to select a configuration, and to narrow approaches. The preliminary design is reported in Section II.

Model design and fabrication followed preliminary design. A description of the selected design, findings of structural, thermal, and weight analyses, and fabrication techniques are discussed in Section III.

Before model delivery, Goodyear Aerospace performed electrical, vibration, bell jar sample, and contour tests. Section IV reports results. Ground deployment operational instructions are reported in Section V.

C. RESULTS

Figure 1 shows the high-gain spacecraft antenna model in the packaged and deployed configurations.

The model was delivered to JPL in April 1964. Black-and-white and color movies of antenna deployment at Goodyear Aerospace have been prepared and delivered.

The antenna design basically consists of curved radial ribs that extend from a hub to the outer periphery to support a reflector screen and establish parabolic contour. The ribs are pivoted at the hub rim and nest circumferentially around the hub rim in the packaged condition. The screen material is a lightweight Invar wire mesh that is attached to the ribs.

Long missions with antenna steering requirements can be met with this approach. Accuracies on the order of ±0.10 inch rms are practicable. Antenna weight is on the order of 0.37 psf with a packaging ratio of 2.4 : 1.

The antenna can be erected and boresighted prior to final packaging and launch.

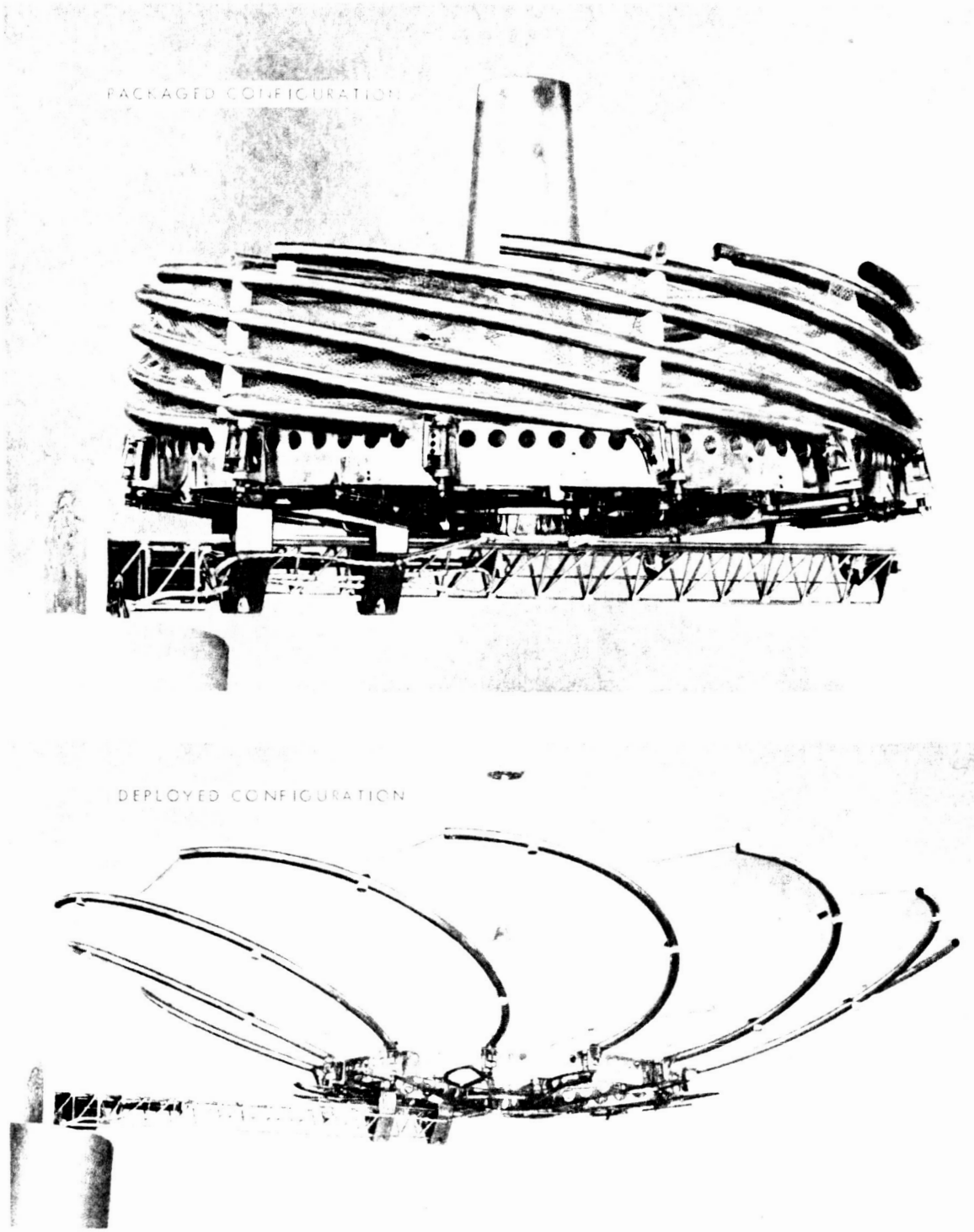

Figure 1. High-Gain Spacecraft Antenna

SECTION II. PRELIMINARY DESIGN AND ANALYSIS

A. GENERAL

The initial task included a preliminary investigation of antenna characteristics, configuration studies, and a study of screening materials. This section describes the preliminary design effort.

B. ANTENNA ELECTRICAL CHARACTERISTICS

The effects of mechanical design parameters on the radiation characteristics of an antenna were investigated. Parameters considered were the number of rib sections, tolerance of the ribs, tolerances in the inner nonfoldable section, outside diameters, and illumination tapers. Primary consideration was given to the gain reduction caused by these parameters. The antenna selected for the preliminary study is a circular paraboloid type consisting of a fixed center hub with outer sections that unfurl. The curved ribs of the unfurlable section rotate into position, providing a singly covered surface between any two ribs as shown in Figure 1. Specification requirements for the antenna were the same as those imposed by JPL and detailed in Section I.

The study indicated that the primary controlling parameters to limit gain reduction for an unfurlable-type antenna is the number of ribs in the deployable section (see Figure 2). The rib tolerance is a second-order effect (see Figure 2), and the center hub tolerance effect is negligible (see Figure 3). The packaging ratio is also a negligible effect for a given antenna size; however, as the over-all deployed diameter is increased, the number of ribs must also be increased (see Figure 4). The complete analysis showing derivations and the specific constraints of this study is given in Appendix A.

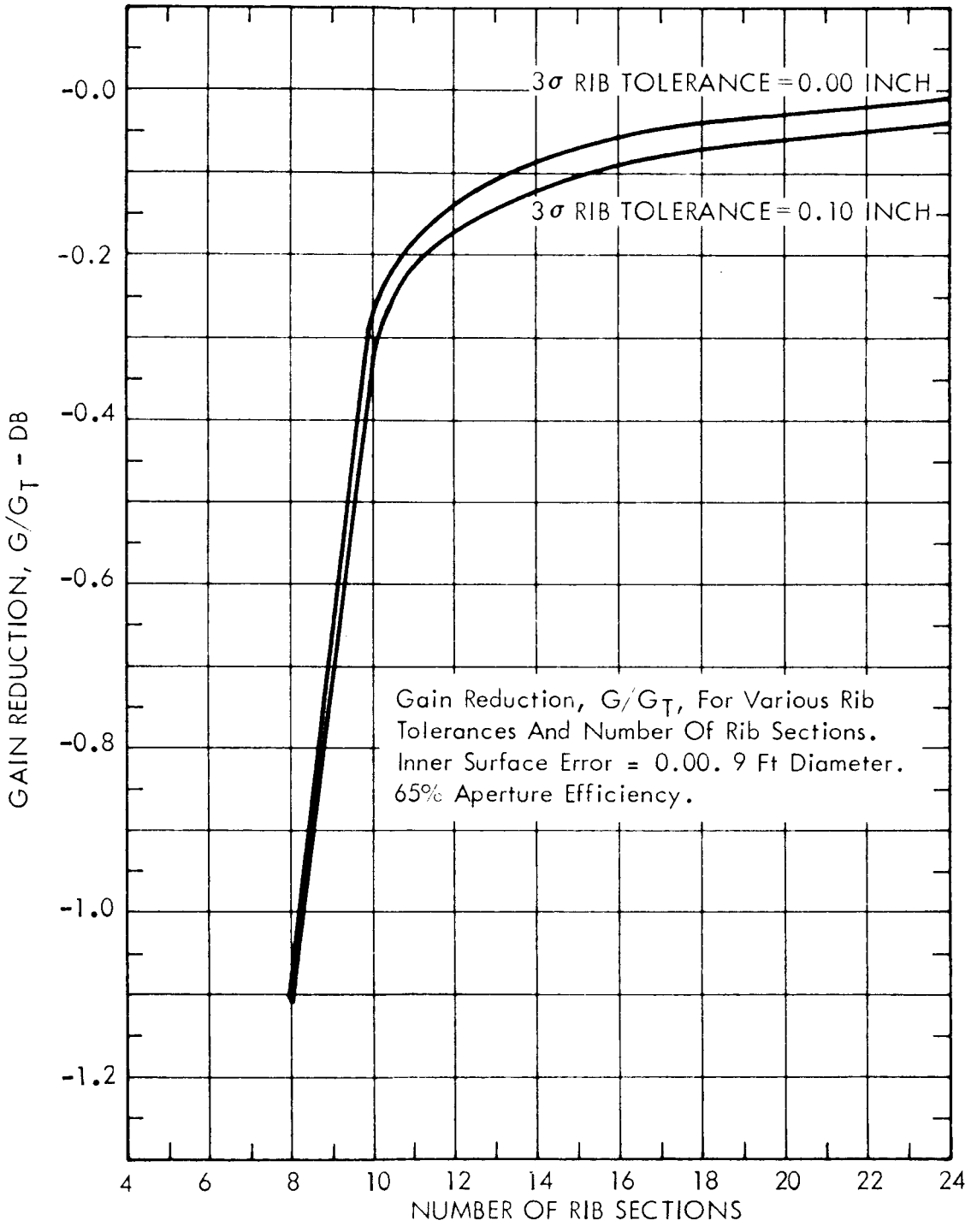

Figure 2. Gain Reduction as a Function of Rib Tolerance

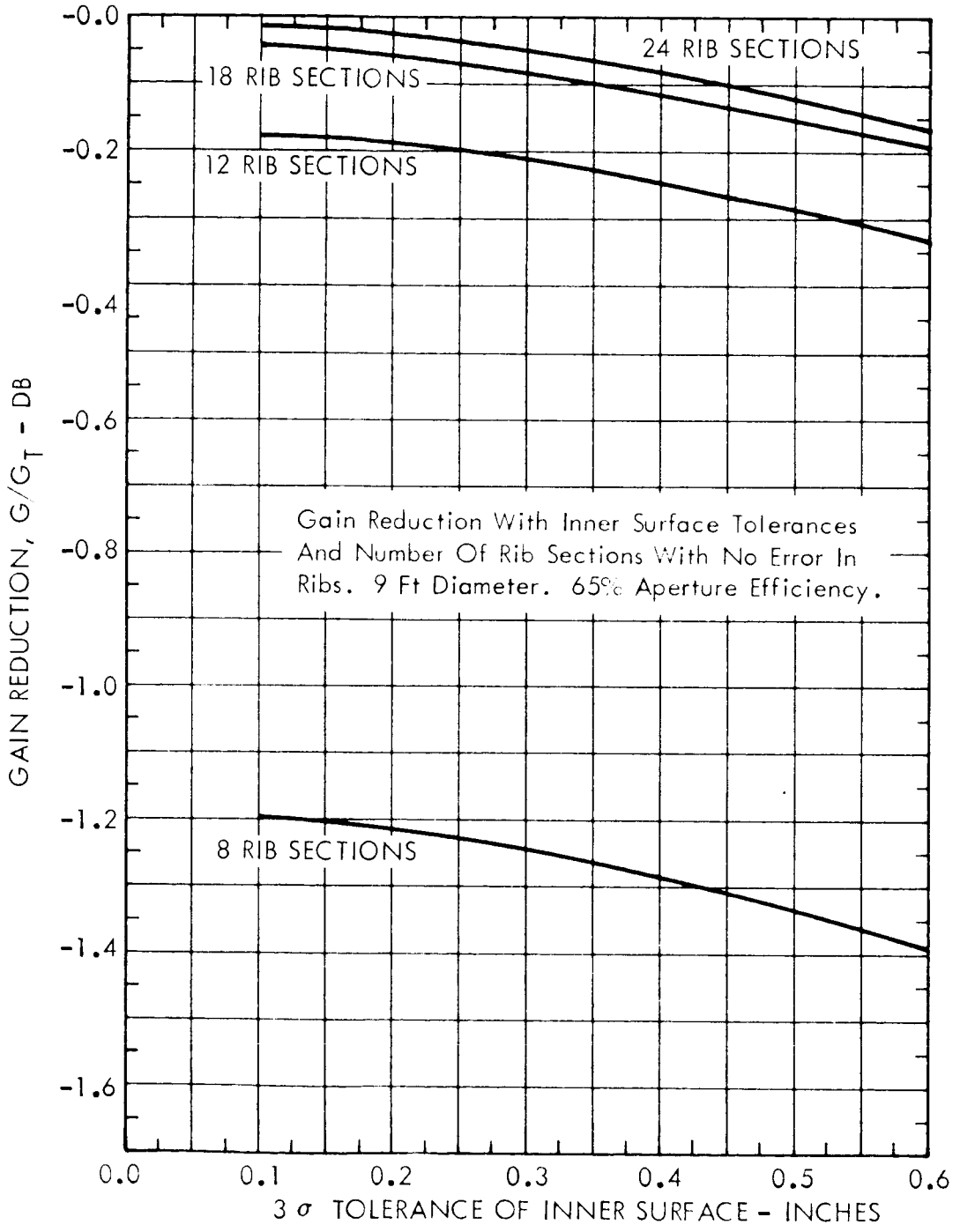

Figure 3. Gain Reduction as a Function of Inner Surface Tolerance

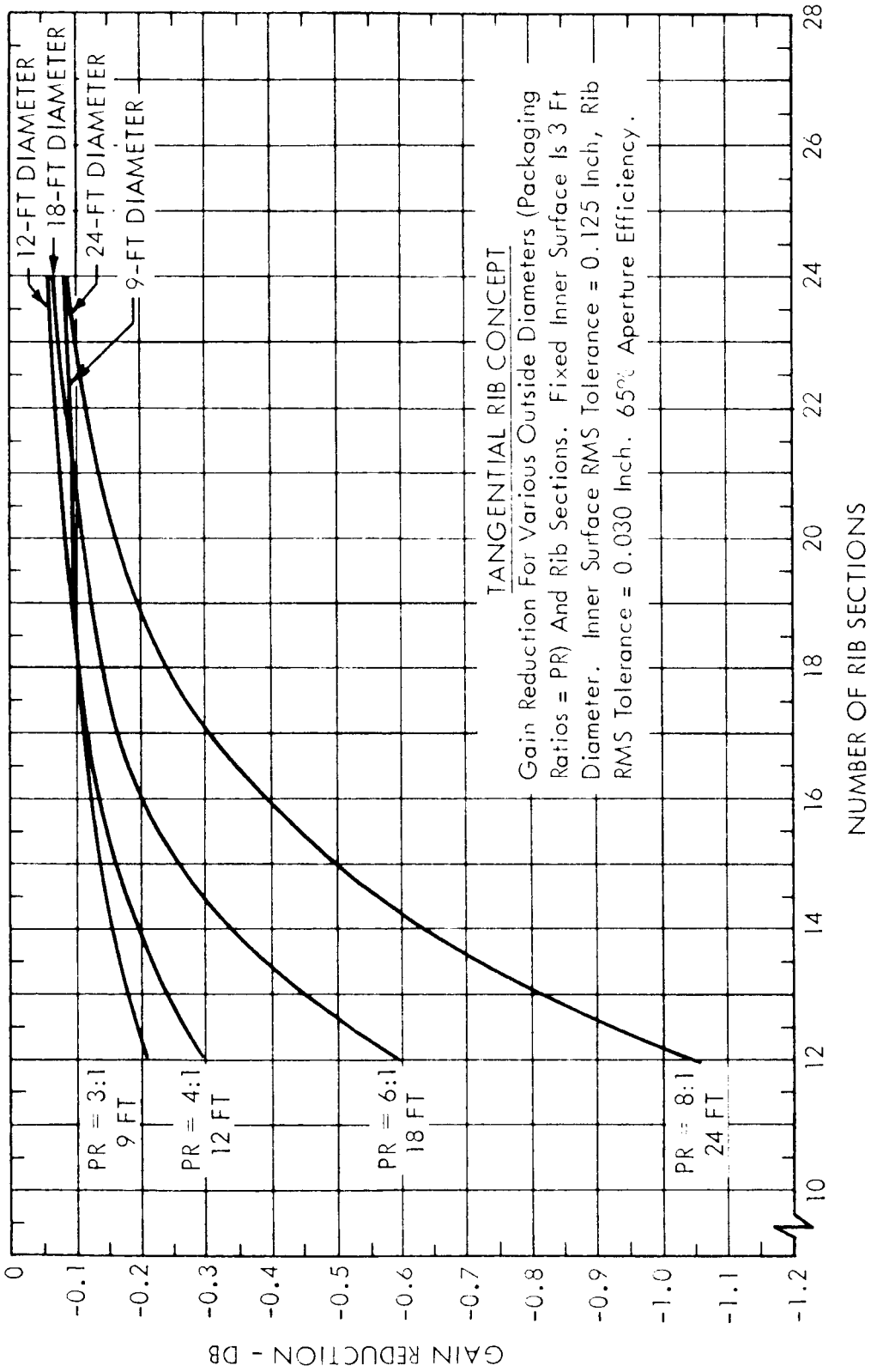

Figure 4. Gain Reduction for Various Outside Diameters and Rib Sections

C. CONFIGURATION STUDIES

Seven antenna configurations were studied at the outset of the program. Relative merits were considered and documented as shown in Table I. Configurations 1 and 7 were believed to be the most feasible; further analysis was accomplished on each, and feasibility models were fabricated. Configuration 1 is shown in Figure 5, and Configuration 7 is shown in Figure 6. The relative weights of these two configurations are given in Figures 7 and 8.

D. MODEL SELECTION

The results of the preliminary design studies were presented to JPL on 18 March 1963, and the following design parameters and objectives were selected for the advanced development model:

(1) Model to be hard rib, hinged, radial (similar to Configuration 7 described in Table I).

(2) Erected diameter of 9 feet.

(3) Hinge diameter of 42 inches.

(4) 12 ribs.

(5) Over-all package diameter of 45 inches.

(6) Erected diameter and package diameter will give a packaging ratio of 2.4: 1.

(7) Arc length of erected elements will be 145 degrees.

(8) Tolerances: 0.1 inch rms error on the center hub section of the antenna, 0.033 inch rms error in the ribs, and a 0.1 inch tip deflection under a 1-g gravitational field.

Table I. Spacecraft Antenna Configurations

Config-uration	Design	Maximum Packaging Ratio (Antenna to Package Diameters)	Relative Complexity	Components Required	Accuracy	Stiffness	Component Manufacture Complexity	Ease of Assembly	Operation	Comments
1	Flexible Rib, tangential attachment, unstressed 	8 to 9	Low	Actuators, tube and rests, swivels, cable and pulley	Rib very good. Mesh very good (See comment 1.)	Hard	Rib difficult	Very easy	Actuator controls rate of opening. (See comments 2 and 3.)	(1) Mesh is not stretched. (2) After opening, actuator unnecessary. (3) Care required in handling rib.
2	Flexible Rib, hinged, radial, unstressed 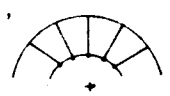	8 to 9	Very high	Same as configuration 1 plus 7.	Rib very good. Clearance at hinge yields error. Mesh fair. (See comment 1.)	Hard axially, fair laterally	Mesh difficult, rib difficult	Fairly easy	Same as Configuration 1 plus second actuator rotates rib about hinge. Must be held open by lock or actuator (See Comment 2.)	(1) Mesh is stretched locally. (2) Care required when handling rib.
3	Flat Flexible Rib, tangential attachment, stressed 	3 to 4	High	Same as Configuration 1 plus cables to keep rib stressed. (See comment 4.)	Rib fair Mesh fair Cable across aperture. (See comment 1.)	Soft (see comment 2)	Rib difficult	Easy	Same as Configuration 1. (See comment 3.)	(1) Mesh is not stretched. (2) Rib will twist when vibrated laterally or axially. (3) After opening, actuator unnecessary. (4) Cannot have a stable rib with only one cable.
4	Flat Flexible Rib, hinged, radial, stressed 	3.5 to 4.5	Very high	Same as Configuration 2 plus cables to keep rib stressed. (See comment 3)	Rib fair Clearance at hinge yields error. Mesh fair Cable crosses aperture (See comment 1.	Soft (see comment 2)	Mesh difficult, rib difficult	Fair	Same as Configuration 2.	(1) Mesh is stretched locally. (2) Rib will twist when vibrated laterally or axially. (3) Cannot have a stable rib with only one cable.
5	Parabolic Bow formed rib, unstressed 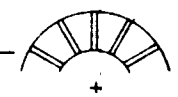		Lowest	Actuator, cables, and drum	Rib very good Mesh very good.	Soft	Rib difficult	Easiest	Actuator controls rate of opening. (See comment 2.)	(1) Mesh is not stretched. (2) Care required when coiling rib. (3) Cannot recover from an elastic buckle.
	Flat Rib, stressed		Low	Same as above plus cable to keep rib stressed to parabolic curve	Rib fair Mesh very good. Cable crosses aperture. See comment 1.)	Soft	Rib difficult	Very easy	Same as above. (See comments 2 and 3.)	
6	Hard Rib, hinged, radial, articulated 	3.5 (No actuator for outboard rib)	Highest	Same as Configuration 7 plus outboard hinge cable to open outboard rib stop	Rib good. Clearance at hinges yields error. Mesh fair. Cable crosses aperture. (See comment 1.)	Hard	Mesh difficult	Most difficult (see comment 2)	Same as Configuration 7 plus tensioned cable opens outboard rib.	(1) Mesh is stretched locally. (2) Hinge angle very critical to allow clearance between ribs when folded. (3) Packaged height is marginal.
7	Hard Rib, hinged, radial 	2.8	High	Actuator, cables and pulleys, drum stop, spring or automatic hinge	Rib very good Clearance at hinge yields error. (See comment	Hard	Mesh difficult	Difficult (see comment 2)	Actuator opens rib. Must be held open by a lock or actuator.	(1) Mesh is stretched locally. (2) Hinge angle very critical to allow clearance between ribs when folded. (3) Packaged height is marginal.

NOTES: 1. Analysis based on package diameter and height specified [illegible]

2. Rate of opening of dish is controlled.

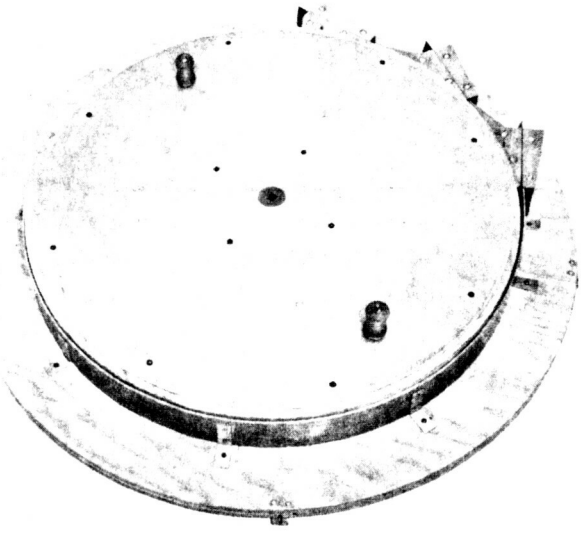

PACKAGED

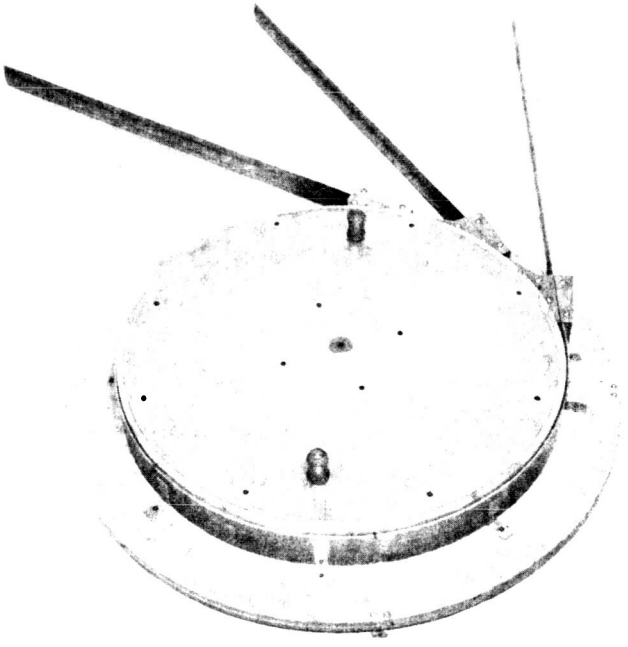

DEPLOYED

Figure 5. Configuration 1

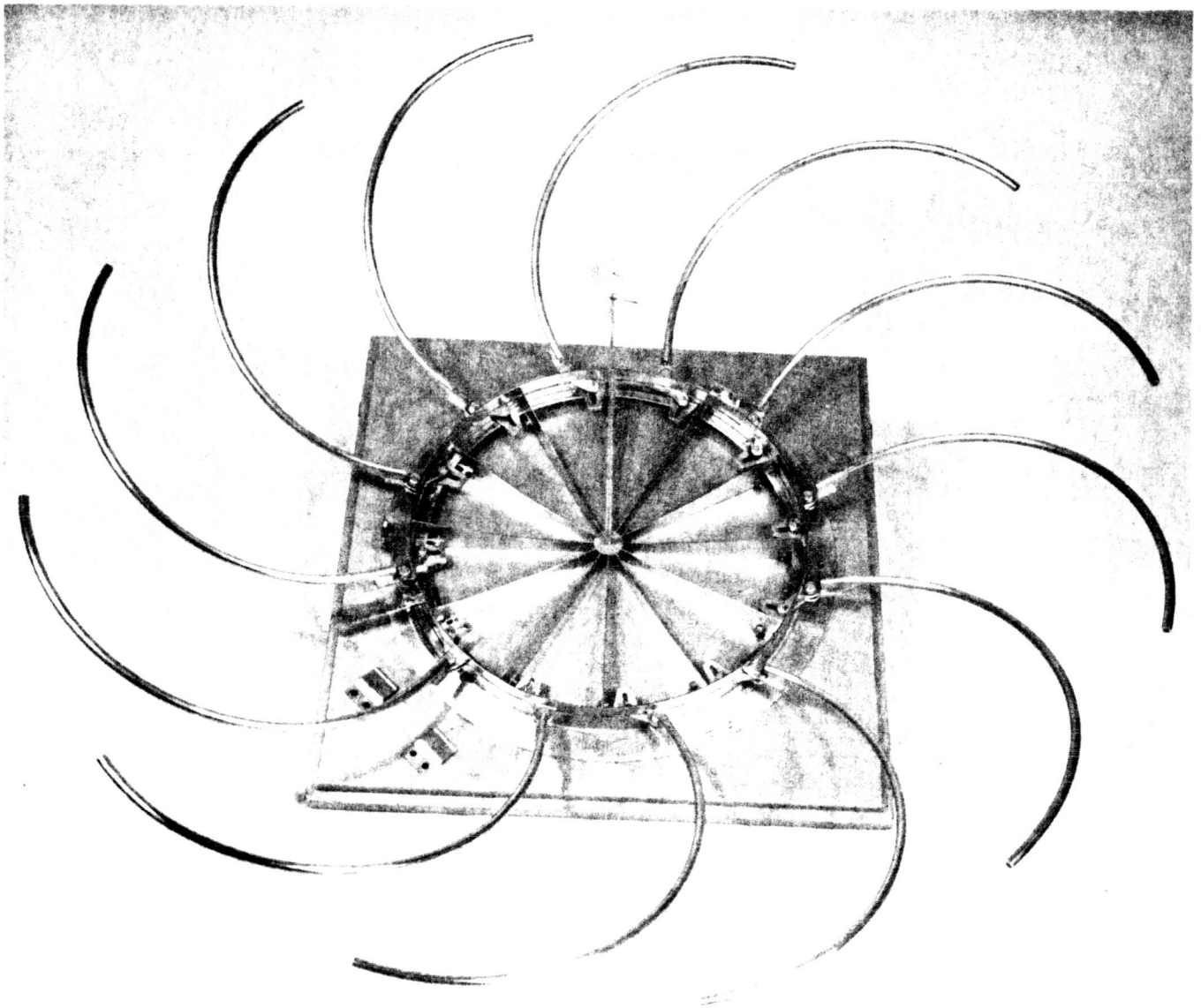

Figure 6. Configuration 7

STAINLESS STEEL
$t/r = 0.00267$
$\theta = 25^{\circ}$
FREQUENCY
SOFT AXIS >1.0 CPS
STIFF AXIS >3.99 CPS
DEFLECTION - RIBS
STIFF AXIS<0.067 IN. AT 1G
STRENGTH - RIBS
STIFF AXIS>3.67G
SOFT AXIS>0.96G
△ ASSUMED MINIMUM GAGE - 0.002 IN.

NOTE: ALL RIB WEIGHTS INCLUDE A 100% CONTINGENCE FACTOR.
HUB WT - 16 LB
SCREEN WT - 0.00495 LB FT^2
HUB DIAMETER - 42 IN.

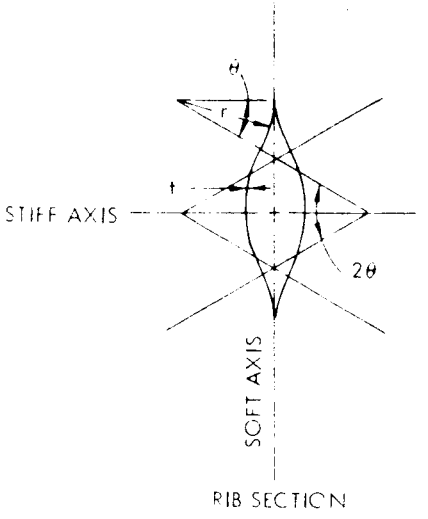

RIB SECTION

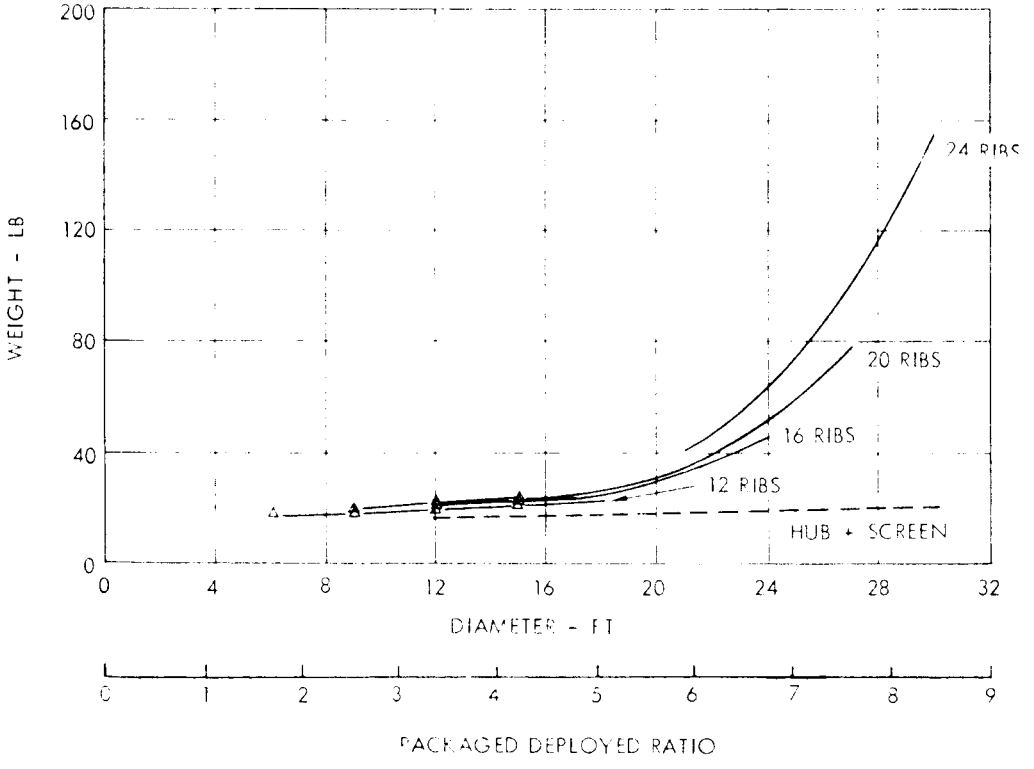

Figure 7. Reflector Weight of Configuration 1

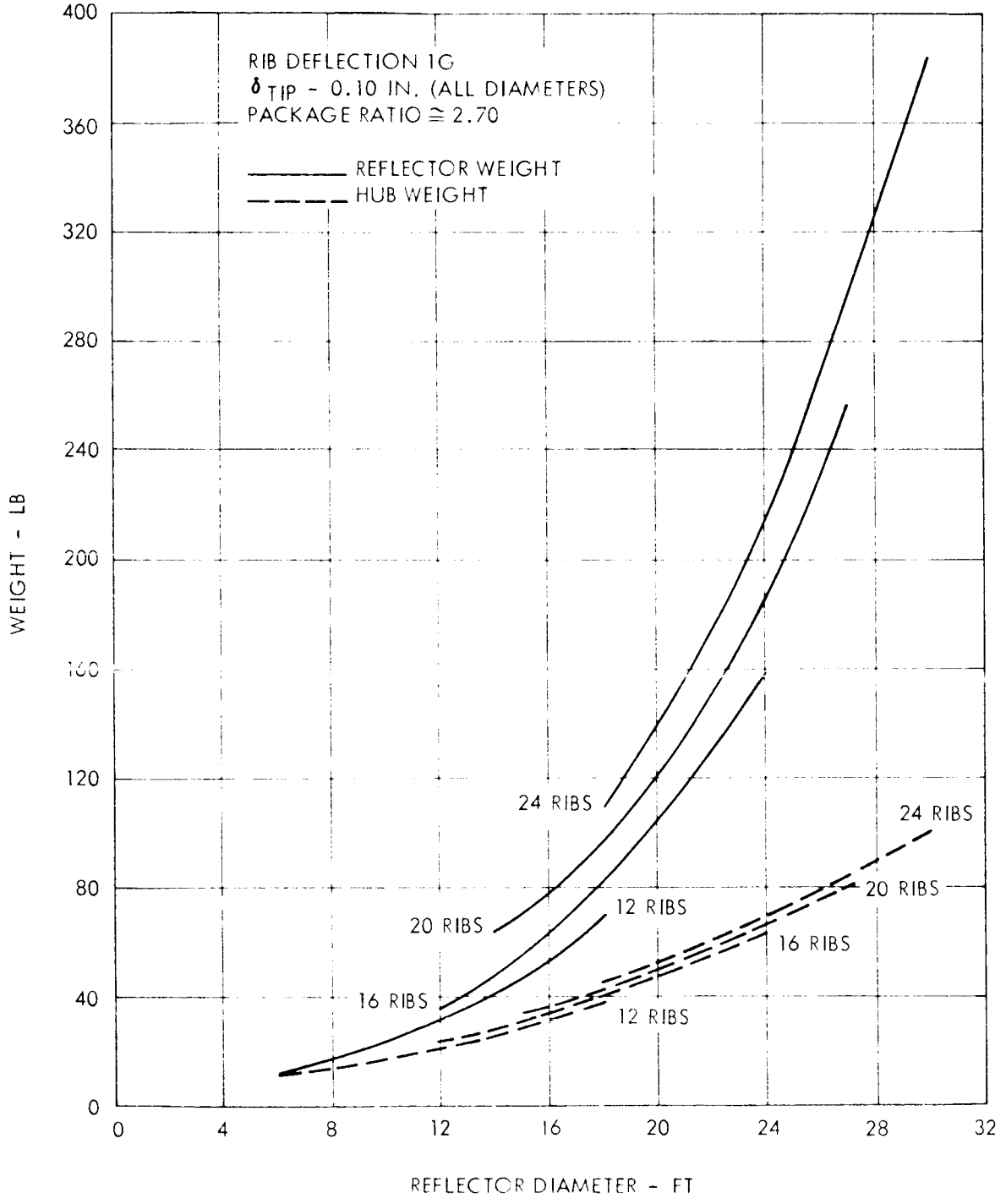

Figure 8. Reflector Weight of Configuration 7

(9) Over-all efficiency loss due to mechanical tolerances and errors resulting from the deviation of the antenna from a true parabolic shape is 0.3 db. In addition, loss will be incurred due to reflectivity loss of the proposed mesh. Total loss should be considerably less than the 0.9-db tolerance of the specification.

E. SCREENING MATERIAL STUDIES

1. General

Fabrication of the antenna reflecting surface from monofilament wire 0.003 inch in diameter in a rectangular weave pattern was initially proposed. A "chicken wire" geometry in which the netting is formed from parallel rows of filaments that are mechanically intermeshed by twisting at regular intervals was slated for investigation. The resulting hexagonal pattern then would be reshaped to a rectangular pattern to provide stiffness in one direction and compliance in the orthogonal direction. The final rectangular mesh netting configuration will provide the flexibility for the packaging operation and will follow the rib contour in the extended configuration while providing the rigidity needed for shape and tolerance.

2. "Chicken Wire" Manufacturers

First contacts with manufacturers of "chicken wire" and wire fencing were not productive. None of the manufacturers had knowledge of the availability of the wire required. None had experience in wire smaller than 20 gage (0.032 inch). Three-quarter inch to one inch mesh gages were found to be standard sizes. It was apparent that a long-term development program by a netting machine manufacturer was necessary if "chicken wire" plans were pursued.

3. In-House Efforts

In an attempt to develop a welding-weaving technique, wires were laid up on a hand frame on 1/8-inch centers. Each cross-over was spot welded and then every

other fill wire was cut in a staggered pattern such that the effect of a rectangular mesh was obtained. A development program appeared necessary to maintain dimensional control of the mesh size, to perform consistent welding of the intersections, and to cut required wires without distortion of the remainder.

Some expanded metal mesh tests were performed. Samples of 0.003 aluminum sheet pierced to have a 0.005 web with an opening of approximately 1/8-inch were placed on a test jig that simulated the furling and unfurling motion proposed for the antenna structure. Although the mesh did not tear, geometry was apparently not sufficient to deflect without yield of the metal at the corners. Manufacturers of the samples were pessimistic about further testing of samples because of the deflections required with a standard diamond pattern. Other configurations would have required additional tooling and development work.

4. Textile Industry

Approximately 30 inquiries were sent to textile mills and colleges in an effort to create interest in this program. Response from manufacturers was not good; however, North Carolina State College expressed an interest in developing the process.

5. North Caroline State College Development Service

The School of Textiles was given a subcontract in early February 1963 to produce a material to Goodyear Aerospace specifications. The quantity of material to be delivered was only that required to determine feasibility on a best effort basis. The basic problem for North Carolina State College was to establish the feasibility of producing the screen material from fine wire to a desired pattern that has high stretch in one direction.

Several samples were produced. First, a 3-mil Invar wire knit was produced on a hand-operated V-bed knitter. The knitter can produce material up to 24 inches

wide. The material produced was a typical rib stretch knit considered a back-up material. The second investigation used a Cidega Machine, which is a type of Raschel. The flat bed of the Cidega can produce material up to 50 inches wide. A straight chain was produced with lay-ins for the cross links which came off from a second warp. One warp was a 3-mil Invar; the others were textile. Cross links were 3-mil Invar. A small sample of the material was obtained. The third sample was from a flat bed Raschel Lace-type Machine. The machine, which can produce material up to 90 inches wide, is a 36 gage machine with 18 needles per inch. A typical fish net pattern was fashioned using Invar wire twisted together with a textile yarn.

Of the three samples, Goodyear Aerospace preferred the straight chain. The rib stretch knit was the second choice. A tighter chain to eliminate the possibility of snagging was considered for the straight chain.

SECTION III. MODEL DESIGN AND FABRICATION

A. GENERAL

The high-gain spacecraft antenna, which describes a 9-foot diameter paraboloid when fully deployed, is designed for Mariner-type interplanetary travel. The primary influences governing antenna design were JPL specifications, which included packaged envelope definition for launch, weight limitation, 1-g environment functional requirements such as contour and electrical axis to boom tolerances, and the spacecraft interface definition, which dictated a deployment boom. Other factors limiting design were selection of materials satisfactory for space environment and state-of-the-art technology.

Figure 1 shows the antenna model in the packaged configuration and in the ground-deployed configuration.

This section describes the antenna design and discusses the structural study, thermal analysis, weight analysis, and fabrication study, which established design parameters.

B. DESCRIPTION

1. [redacted]

The packaged antenna consists basically of a reflector, an RF feed and feed support assembly, an antenna deployment system, a deployment boom, and a jettisonable packaging canister.

2. Reflector

a. General. The reflector, approximately 9 feet in diameter when deployed, packages to a maximum diameter of 43 inches. The reflector consists of a

hub structure that supports the 12 curved radial ribs and an orthotropic, plated Invar, Raschel lace-styled screen.

b. Hub. The hub (see Figure 1) is a conventional structural arrangement approximately 41.38 inches in idameter. The hub serves as a fixed center portion of the parabolic dish, is the structural interface between the feed support and jettisonable packaging canister, is the structural pickup of the deployment boom, and supports much of the deployment system. Hinge brackets are located 30 degrees apart on the outer periphery of the hub. The hinge brackets, inclined toward the hub center, receive the curved radial ribs.

c. Curved Radial Ribs. When packaged, the curved radial ribs (see Figure 1) nest circumferentially about the hub. Each rib consists of a 0.007-inch wall x 1-inch OD, curved Invar tube welded at the hinge end to a bracket. A hinge pin bracket is assembled on the welded bracket. The hinge pin bracket is mated to the hinge bracket with a combination bushing and tapered nut. The ribs extend 33 inches from the hinge brackets to the outer periphery to form the parabolic contour and to support the orthotropic screen.

d. Orthotropic Screen. The 3-mil diameter wire orthotropic screen (see Figure 1) is attached to the hub and ribs with an epoxy of 60 percent Epon 828 and 40 percent Versamid 125. The screen, when packaged, folds inward over the hub without undue stress because of its orthotropic characteristics.

3. RF Feed and Feed Support Assembly

The electrical feed assembly (see Figure 1) is installed on the geometric axis of the hub structure. The electrical feed assembly includes a telescoping RF feed unit with an outer housing that contains the extension bellows mounted to the unexposed section of the feed, a gas expansion and combination coaxial cable storage chamber, coaxial cable, and associated plumbing connected to an explosive

actuated gas energy release unit (Eager Pak, Conax Corp, Buffalo, N.Y.). Except for the extension bellows, RF feed, and feed extension lock springs, the feed assembly components are manufactured entirely from Invar sheet stock. The extension bellows is made of nylon cloth treated with polyurethane resin, the feed is made of aluminum alloy tubing, and the feed extension lock springs are made of a copper-beryllium alloy.

4. Deployment System

a. General. Basically the deployment system (see Figure 9) consists of a 13.25-inch diameter drive drum, deployment quadrants, alignment pulleys, cabling, and a traversing carriage.

b. Drive Drum. The drive drum, located below the center of the parabolic contour surface of the hub structure, is grooved to receive the drive and the quadrant cables.

c. Deployment Quadrants. A magnesium deployment quadrant is attached to the hinge pin bracket of each curved radial rib. The drive cables are attached to each quadrant over an alignment pulley, and to the drive drum.

d. Traversing Carriage. The traversing carriage, located on the bottom of the hub structure, consists of roller bearings and triangular-shaped structural members.

5. Deployment Boom

The deployment boom (see Figure 1) is fabricated from aluminum alloy and is essentially a triangularly trussed welded structure with longitudinal grooved tracks located at the vertices of the triangular structure. The boom structure houses a 28 VDC, 10 ampere driven ball screw-type actuator, drive cable pulleys, and alignment fixtures for packaging and deployment of the antenna.

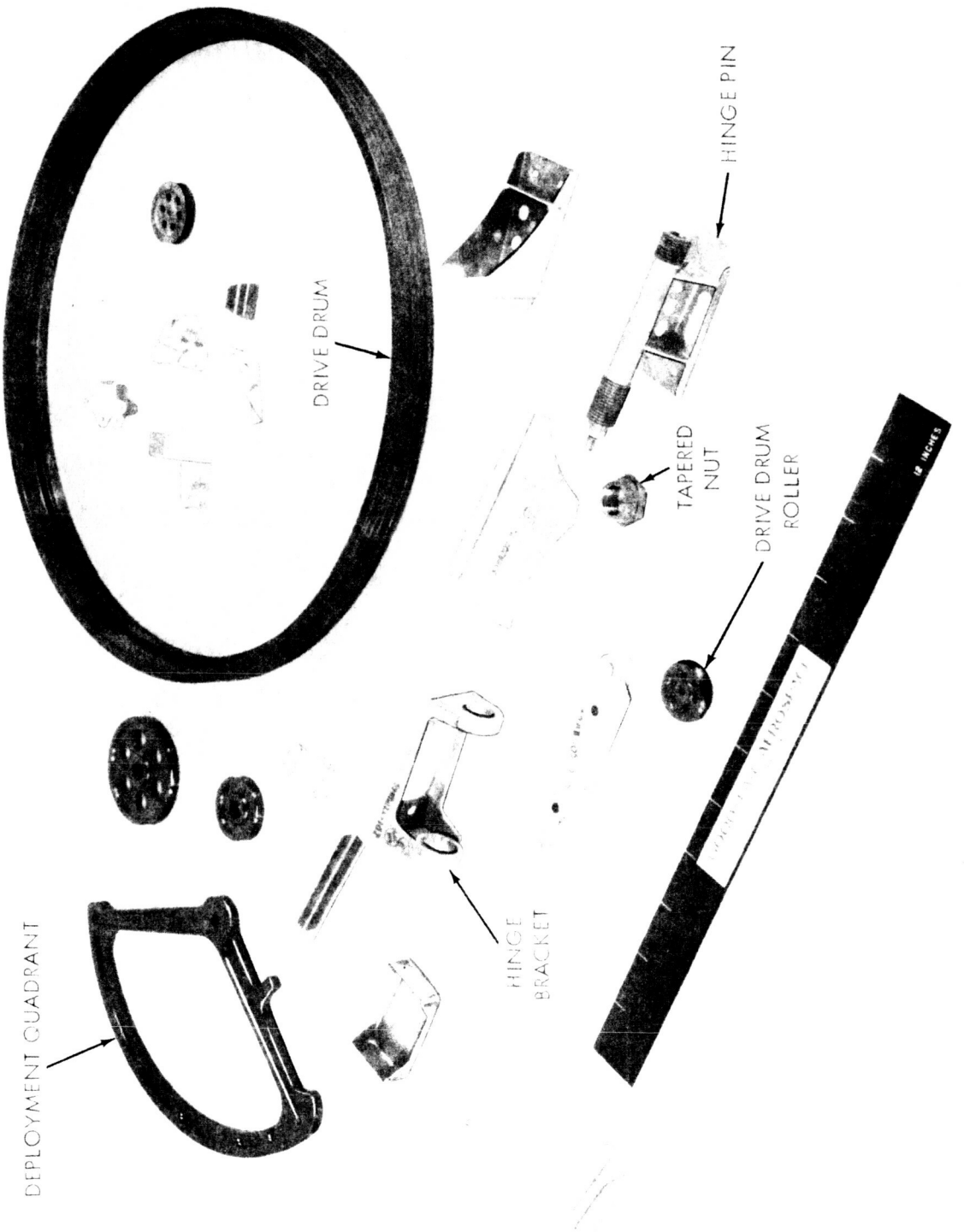

Figure 9. Typical Antenna Components and Hardware

6. Jettisonable Packaging Canister

The jettisonable packaging canister (see Figure 1) is primarily intended to protect the packaged antenna against damage resulting from shock loads and vibrations encountered during launch and escape velocities. The canister consists of a cone and six rib support arms with piano wire tension supports. The canister is basically a fiberglass laminate incorporating metal reinforcements at the package tie-down points.

C. DEPLOYMENT

1. Canister Separation

Three threaded adapters on the hub match the canister tie-down points. In each adapter is a 6071 pin pusher (McCormick-Selph Associates, Hollister, California) with externally-threaded housings. A shouldered screw stem that engages the mating holes in the canister projects from the housing. Self-locking nuts secure the canister to the pin pusher. Each pin pusher is armed with a threaded Mk 54 Mod 0 igniter (McCormick-Selph Associates). Application of 28 VDC, 10 ampere power fires the igniters, and the resultant gas energy jettisons the shouldered pins and canister away from the antenna, completely exposing the retracted feed.

2. Feed Extension

When 28 VDC, 10 ampere power is applied to trigger an explosive charge in the explosive actuated gas energy release (Eager Pak, Conax Corp, Buffalo, N.Y.), a disc ruptures to allow 2.6 cubic inches of stored 500-psi nitrogen gas to escape through a plumbing system into the gas expansion chamber. Increasing gas pressure in the expansion chamber extends a bellows which, in turn, extends the feed through the feed support outward until extension lock springs engage slotted holes in the feed support, limiting the feed to a specific extension length.

3. Antenna-Boom Separation

The reflector hub traversing undercarriage structure includes two triangular-shaped brackets. Each bracket contains three roller bearings that ride in the longitudinally-grooved tracks of the boom. In the packaged configuration, two lugs in the bracket nearest the spacecraft interface mate and engage the No. 4072 ball releases (McCormick-Selph Associates) on the boom to secure the reflector to the boom. Each ball release is armed with a threaded Mk 54 Mod 0 igniter. Electrical power applied to the antenna-boom separation cable assemblies fires the igniters and drives a piston forward within each of the ball releases, allowing the balls to drop flush with the ball release housing. The lugs on the reflector hub traversing undercarriage are then free to pass over the ball releases.

4. Antenna Deployment

When power is applied to the screw-type linear actuator, the actuator retracts and pulls the antenna reflector traversing cable, which is routed over a pulley arrangement providing four inches of cable travel for every one inch of actuator travel. As the actuator retracts, the reflector traverses outward along the boom. Simultaneously the drive drum cable, attached to the deployment boom and to the drive drum, pulls free of breakaway ties until 9.50 inches of slack is taken up. Then the drive drum cable rotates the drive drum and the drum, in turn, receives windings of deployment quadrant cables. As the quadrant cables wind about the drive drum, the quadrants, fixed to the hinge pin brackets, rotate and move the curved radial ribs outward to form the parabolic contour of the reflector. During deployment, the actuator retracts approximately 7.50 inches while the reflector traverses 30 inches on the boom. Limit switches control actuator extension and retraction. At the fully deployed configuration, the reflector is secured on the boom by two leaf-spring locks.

D. STRUCTURAL STUDY

Load conditions for the 9-foot antenna design were derived from loads in JPL Specification 30257. For the packaged antenna under various conditions the loads were as follows:

(1) 12.69 g's along boom axis toward base. 5.92 g's along parabola axis away from boom.

(2) 3.72 g's along boom axis away from base. 1.69 g's along parabola axis toward boom.

(3) 6 g's along elevation axis.

(4) 2.54 g's along boom away from base. 5.44 g's along parabola axis away from boom.

The packaged antenna is to survive the vibration environment of Specification 30257.

Design loads for deployment evolved over the period of deployment system design were as follows:

(1) Ultimate actuator load - 1600 pounds

(2) Maximum antenna drive cable load - 400 pounds ultimate

(3) Maximum drive drum cable load - 360 pounds ultimate

(4) Maximum quadrant cable load - 81 pounds ultimate

Limit loads are 2/3 of ultimate loads and the stresses from the limit loads are to be less than the yield strength of the material.

The design condition for the deployed antenna is a natural frequency of more than 1 cps. Attenuation offered by the structure to the other loads of JPL Specifications reduce the loads to a noncritical level. The deflection of the curved radial ribs is not to exceed 0.13 inch in a 1-g environment.

Physical properties of the Invar (Reference 1) used in construction of the antenna are as follows:

(1) Ultimate Tensile Strength (F_{tu}) $\geq$ 40,000 psi

(2) Tensile Yield Strength (F_{ty}) $\geq$ 24,000 psi

(3) Young's Modulus (E) = 22×10^6 psi

Allowable stress for other materials used in the antenna are from Reference 2.

The boom, a welded aluminum truss, was analyzed using a graphical technique. Stresses in the 6061 T6 aluminum were limited to 8000 psi for the design loads. Nominal section areas were used in the stress calculations.

Crippling allowable for Invar sheet metal components was obtained by noting similarity in Invar yield and ultimate tensile strengths to those of annealed 18-8 stainless steel. It was assumed that the crippling stress of Invar would therefore be proportional to the modulus ratio of the materials, i.e.,

$$F_{CC\ (Invar)} = \frac{E_{\ Invar}}{E_{\ (18-8)}} F_{CC\ (18-8)}. \qquad (1)$$

The sheet metal elements are formed to have typical sections as shown in Figure 10. The effective cap area is assumed to be that of the corner angle dimensioned in detail in Figure 10. It may be noted that the corner angle is composed of a flat element with one edge free, a flat element without a free edge, and a curved element without free edges. Each flat element is 0.31 - 0.065 - t inch wide, and the curved element radius is 0.065 + (t/2). The modulus ratio is

$$\frac{E\ (Invar)}{E\ (18-8)} = \frac{21}{29} = 0.725\ . \qquad (2)$$

For components 0.012-inch thick, using b for the flat element width and r for the curved element radius (Reference 3),

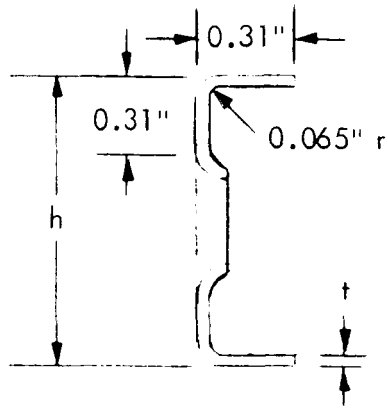

Figure 10. Typical Sheet Metal Element Section

$$\frac{b}{t} = \frac{0.31 - 0.065 - 0.012}{0.012} = \frac{0.233}{0.012} = 19.4 \quad (3)$$

and

$$\frac{r}{t} = \frac{0.065 + (0.012/2)}{0.012} = \frac{0.065 + 0.006}{0.012} = 5.9\ . \quad (4)$$

Where crippling stress exceeds the yield stress, the yield stress is used as the allowable stress. The allowable load on a 0.012-inch thick cap is 146 pounds, as shown by

	b/t or r/t	$F_{CC(18-8)}$	F_{CC}	Area (in.^{2})	P_{CC}
Flat element, one edge free	19.4	25,000	18,000	0.0028	51.7
Flat element, no edge free	19.4	57,000	24,000	0.0028	67.2
Curved element, no edge free	5.9	120,000	24,000	0.00113	27.1
					146.0

For components 0.015-inch thick,

$$\frac{b}{t} = \frac{0.31 - 0.065 - 0.015}{0.015} = 15.3 \quad (5)$$

and

$$\frac{r}{t} = \frac{0.065 + 0.0075}{0.015} = 4.74\ . \quad (6)$$

The allowable cap load on a 0.015-inch cap is 195 pounds, as shown by

	b/t or r/t	$F_{CC(18-8)}$	F_{CC}	Area (in.^{2})	P_{CC}
Flat element, one edge free	15.3	29,000	21,000	0.0036	75.6
Flat element, no edge free	15.3	70,000	24,000	0.0036	86.4
Curved element, no edge free	4.74	120,000	24,000	0.00135	32.4
					194.4

Rivet allowable loads were found by assuming that values in Reference 3 for annealed stainless steel were applicable for Invar sheet, F_{BR} = 150,000 psi for 18-8 annealed. Using the value as an estimate for Invar with an e/D ≥ 2,

Rivet Dia	D/0.012	D/0.015	$P_{0.012}$	$P_{0.015}$
1/16	5.2	4.2	113	140
3/32	7.8*	6.25*	167*	208*

The longest radial hub rib is 18.5 inches long by 0.012 inch thick. The estimated load at the tip is 2 pounds, and the design g-load is 5.92. The centroid-to-centroid distance of the caps is 1.9 inches. A 1.15 factor is used with the crippling allowable, so

$$P = \frac{1.15\ (2)\ (5.92)\ (18.5)}{1.9} = 132 \text{ pounds} \tag{7}$$

$$MS = \frac{146}{132} - 1 = \underline{\underline{0.10}}\ . \tag{8}$$

The deflection equation for a curved tube is developed in Reference 4. Deflection is normal to the plane of the tube.

*Bearing values for D/t greater than 5.5 are to be substantiated by testing. Since no less than two rivets are used in any connection, the maximum required bearing strength is 74 pounds for 0.012-inch material and 97 pounds for 0.015-inch material. The bearing allowables asterisked are deemed safe by inspection.

$$\delta = \frac{\gamma R^4}{Er^2}\left[2\left(\beta + 1 - \cos\beta - \frac{\sin 2\beta}{2}\right) + 2.5\left(\frac{\beta^2}{2} - \beta\sin\beta + \frac{\sin^2\beta}{2}\right)\right] \quad (9)$$

Using Invar, $\gamma = 0.29$ lb/in.^{3} and $E = 22 \times 10^6$ psi, and for the antenna configuration, $R = 21$ inches, $r = 0.5$ inch, $\beta = 140$ degrees.

Therefore,

$$\delta_{tip} = \frac{(0.29)(21)^4}{22 \times 10^6 (0.5)^2}\left\{2\left(\frac{140}{180}\pi + 1 - \cos 140 - \frac{\sin^2 140}{2}\right) + 2.5\left[\left(\frac{140\pi}{180}\right)^2 \frac{1}{2} - \frac{140}{180}\pi\sin 140 + \frac{\sin^2 140}{2}\right]\right\}$$

$$= 0.01028\left[2(2.42 + 1 + 0.766 - 0.206) + 2.5(2.92 - 1.56 + 0.206)\right]$$

$$= 0.01028\,(7.96 + 5.63)$$

$$= 0.1395 \text{ inch.} \quad (10)$$

The tubes will deflect approximately 0.14 inch from their own weight under a 1-g influence.

E. THERMAL ANALYSIS

Temperature analyses have been performed on the antenna ribs, feed, and feed support to assist in the evaluation of thermal deformations. Temperature differentials across the ribs and feed support were found to cause significant distortions unless suitable corrective measures are taken. The following corrective measures were used in the design:

(1) Use of Invar as the structural material. Invar has a low coefficient of expansion, i.e., 0.5×10^{-6} in./in.-^{o}F versus 12×10^{-6} in./in. -^{o}F for aluminum, 7×10^{-6} in./in.-^{o}F for steel.

(2) Use of a protective thermal coating on these items. The external coating selected is an aluminized silicone paint with approximate values of 0.22 for solar absorptance and 0.24 for emittance. The coating will also prevent excessive temperatures on the coated items.

The thermal schematic of the rib configuration used for this analysis is shown in Figure 11. The rib is considered as a cylinder that is divided into eight nodes, each describing an arc of 45 degrees. Three of the nodes are redundant due to symmetry, so that the effective number of nodes is five.

The interior of the rib tube may or may not be occupied by a foam with a density in the order of 4 pcf. In the case of the former, conduction occurs across the foam; in the latter case, internal radiation occurs. A comparison of the foam and Invar thermal conductivities and rib geometries indicates that foam conduction between nodes is approximately 15 percent that of the Invar tube.

The thermal representation of the feed and feed support is shown in Figure 12. The support consists of two thermally distinct sections, i.e., approximately 15.3 inches of the outer housing enclosing the extension bellows and approximately 3.8 inches of the outer housing enclosing the extension guide, which in turn encloses the extension bellows. These sections are also divided into nodes as shown in Configuration 1 of Figure 12. The antenna feed is shown in Configuration 2 of Figure 12.

Several conclusions may be made concerning temperatures:

(1) The temperatures depend upon the orientation of the cylinders with respect to the sun. Temperatures and temperature differentials are maximum when the cylinder is normal to the sun's rays and decrease as the cylinder is pointed toward the sun. For the normal orientation, the average temperatures depend on the ratio of solar absorptance to

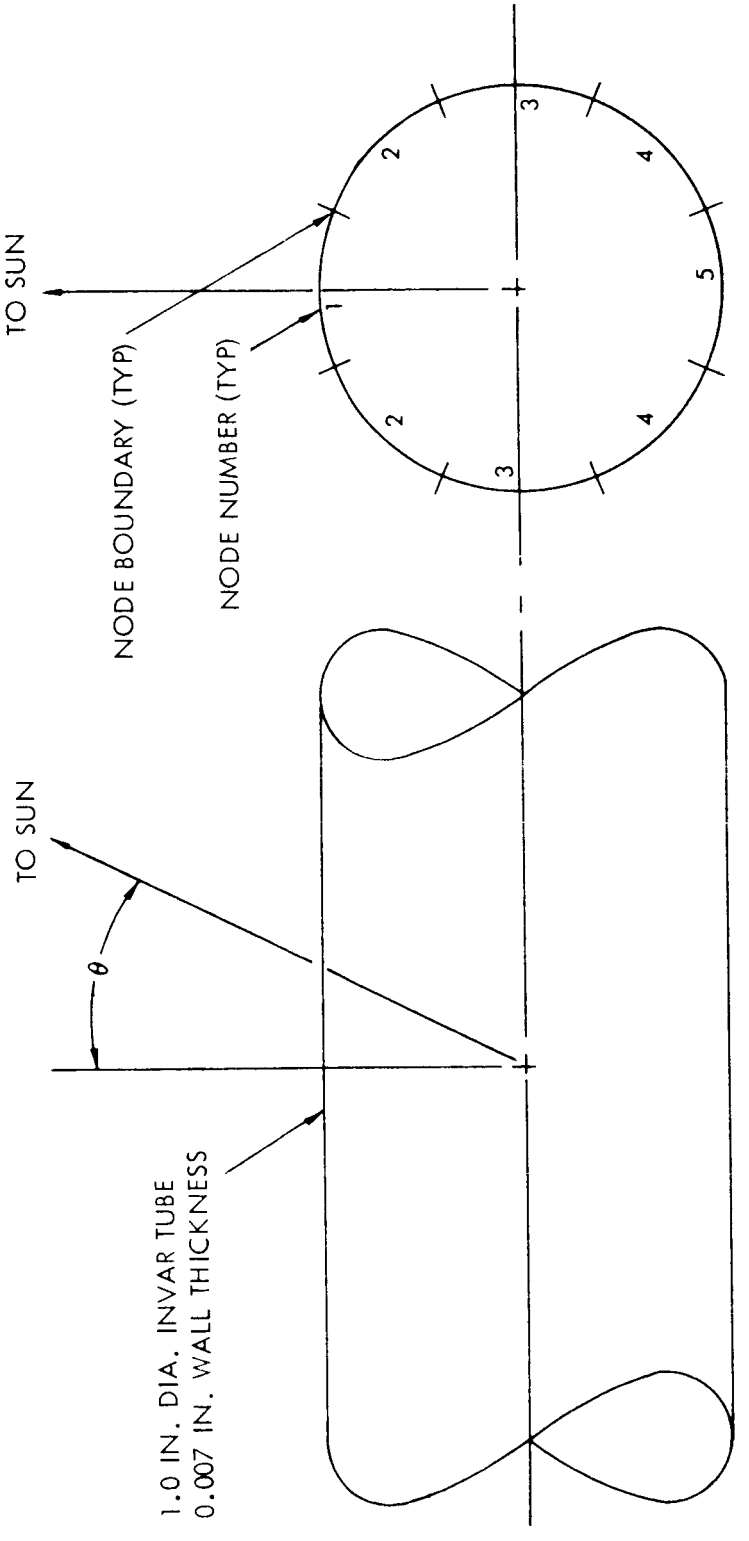

Figure 11. Thermal Schematic of JPL Antenna Ribs

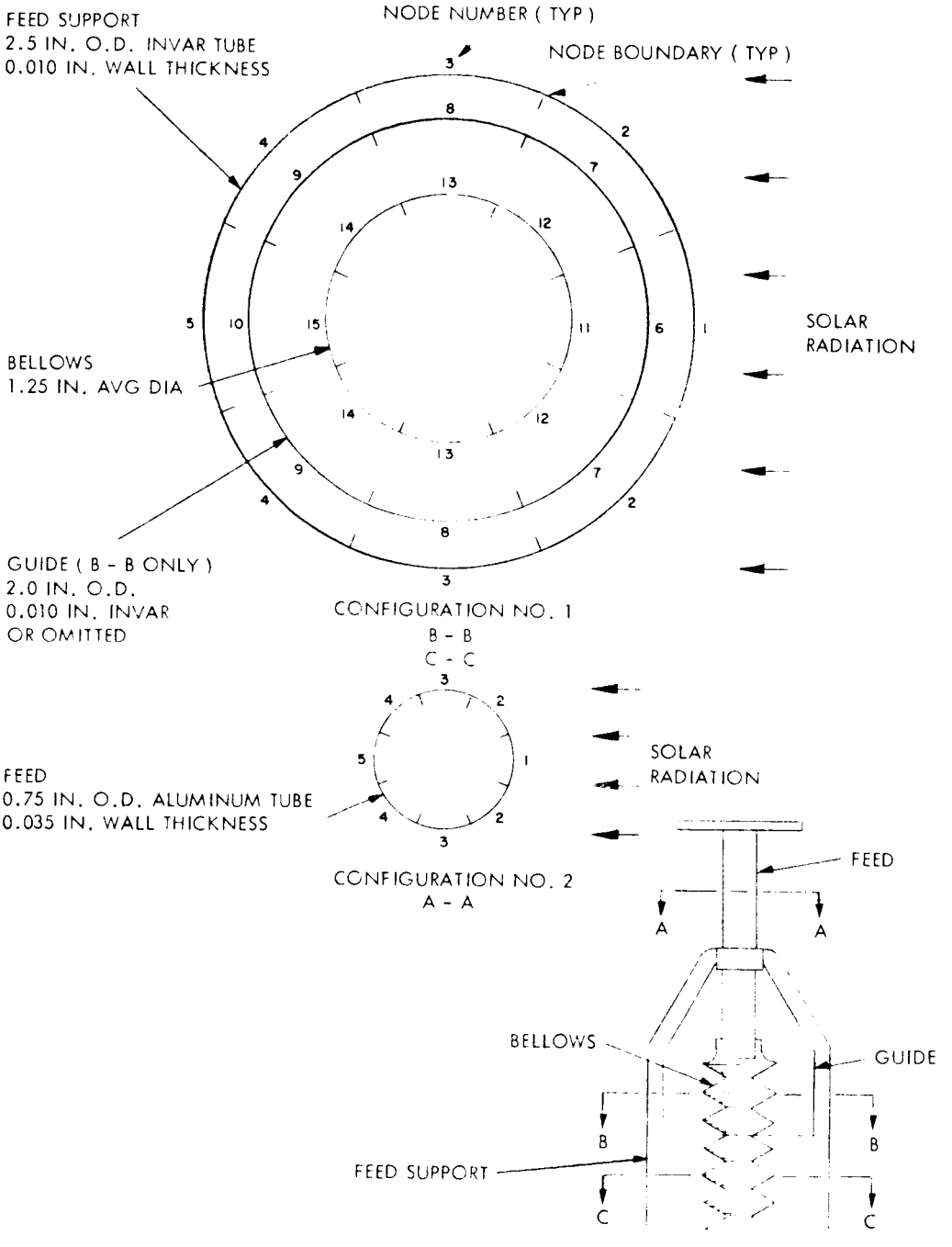

Figure 12. Thermal Schematic of JPL Antenna Feed and Feed Support

emittance (α/ϵ_{ext}) of the external surface of the outer tube. For temperatures in the order of room temperature, this ratio should be approximately unity. When the tubes are pointed toward the sun, very low temperatures will result, possibly in the order of -360°F. Normal orientations are assumed for this analysis unless otherwise stated.

(2) Internal radiation tends to reduce temperature differentials. For this reason, all surfaces other than the external surface of the outer tube should have a high emittance. It is assumed that all internal metal surfaces are painted black so as to have an emittance of 0.9, while the bellows has an emittance of 0.8.

(3) External radiation tends to increase temperature differentials. It is desirable to have the solar absorptance and emittance of the external surface of the outer tube as low as possible. This conclusion coupled with the above conclusion that the (α/ϵ_{ext}) ratio should be approximately unity points to the use of an aluminized silicone paint on the outer surface. Values of 0.22 for solar absorptance and 0.24 for emittance for this paint are assumed for this analysis.

Heat transfer occurs by conduction around the metal tubes and radiation from external and internal surfaces. Each tube was divided into 8 nodes or reference points, each describing an arc of 45 degrees, as shown in Figures 11 and 12. Since the vehicle is exposed only to solar radiation, the tube temperature distributions are symmetrical; five nodes will therefore define the temperature distribution on each tube. A heat or energy balance on each node takes the form:

$$\sum_{n=1}^{n=m+1} \epsilon_n A F_n \sigma (T^4 - T_n^4) + \sum_{n=1}^{n=m} U_n (T - T_n) = CAp\alpha \qquad (10)$$

where

A = surface area of node - ft^2,

Ap = surface area projected and exposed to sun - ft^2,

C = solar constant (442.4 at 1 AU, 845.6 at 0.7233 AU) - $BTU/hr\text{-}ft^2$,

F_n = radiation view factor to indicated node,

m = total number of nodes in system,

m+1 = outer space with a temperature of essentially zero,

n = node number,

T = temperature of node - ^oR,

T_n = temperature of indicated node - ^oR,

U_n = thermal conductance to node n - $BTU/hr\text{-}ft\text{-}^oR$,

α = solar absorptance of external surface,

ϵ_n = effective emittance to indicated node,

σ = Stefan-Boltzmann constant (0.1714×10^{-8}) - $BTU/hr\text{-}ft^2\text{-}^oR^4$.

By determining the coefficients in Equation 10, i.e., $\epsilon_n AF_n$, U_n, and $CA_p\alpha$, for each node, a set of m nonlinear equations involving m temperatures will be obtained. Simultaneous solution of these equations will produce the node temperatures.

To obtain effective emittances and radiation view factors, the tubes are assumed to be infinite in length. All parameters in Equation 10 are fixed by the specified configurations and the above assumptions. The resultant nonlinear simultaneous equations were solved by means of an IBM 1410 Digital Computer. The results are given in Tables II, III, and IV. The astronomical units represent distance from the sun, with a value of 0.7233 indicative of a Venus probe, unity a probe near the earth's orbit but not near the earth, and 1.5237 a Mars probe. The external coatings presumed are bare Invar (approximate values $\alpha = 0.54$, $\epsilon = 0.27$) and aluminized silicone paint ($\alpha = 0.22$, $\epsilon = 0.24$). Use of coatings other than those

Table II. Antenna Rib Temperatures

TUBE	α	ϵ	ASTRONOMICAL UNITS	θ (deg)	NODE NUMBER TEMP (^{o}F)*					$T_1 - T_5$ (^{o}F)
					T_1	T_2	T_3	T_4	T_5	
Foamed	0.54	0.27	1	0	222	205	169	145	138	84
Unfoamed	0.54	0.27	1	0	207	195	170	157	154	53
Either	0.54	0.27	1	90	-320	-320	-320	-320	-320	0
Foamed	0.22	0.24	1	0	84	77	61	50	47	37
Unfoamed	0.22	0.24	1	0	80	74	61	53	51	29
Either	0.22	0.24	1	90	-345	-345	-345	-345	-345	0
Foamed	0.22	0.24	0.7233	0	193	179	150	131	125	68
Unfoamed	0.22	0.24	0.7233	0	181	171	151	140	137	44
Either	0.22	0.24	0.7233	90	-313	-313	-313	-313	-313	0
Unfoamed	0.22	0.24	1.5237	0	-27	-30	-37	-41	-42	15
Foamed	0.22	0.24	1.5237	0	-26	-30	-37	-42	-43	17
Foamed	0.22	0.24	1.5237	30	-42	-45	-52	-56	-57	15
Foamed	0.22	0.24	1.5237	60	-98	-100	-104	-106	-107	9
Foamed	0.22	0.24	1.5237	75	-155	-156	-158	-159	-159	4
Foamed	0.22	0.24	1.5237	80	-184	-185	-186	-187	-187	3
Foamed	0.22	0.24	1.5237	85	-228	-229	-230	-230	-230	2
Foamed	0.22	0.24	1.5237	88	-276	-276	-277	-277	-277	1
Either	0.22	0.24	1.5237	90	-376	-376	-376	-376	-376	0

NOTES: K_{Invar} = 73.2 BTU-in./hr-ft^2-^{o}F.

K_{foam} = 0.2 BTU-in./hr-ft^2-^{o}F.

Internal emittance = 0.9.

*See Figure 11.

Table III. Feed Support Temperatures

Cross Section	Astronomical Units	Node Number Temp (^{O}F)*															$T_1 - T_5$ (^{O}F)
		Feed Support					Guide					Bellows					
		T_1	T_2	T_3	T_4	T_5	T_6	T_7	T_8	T_9	T_{10}	T_{11}	T_{12}	T_{13}	T_{14}	T_{15}	
Guide Omitted (Section C-C of Fig. 12)	1	105	89	55	35	30	--	--	--	--	--	82	75	61	52	50	75
	0.7233	212	191	142	117	109	--	--	--	--	--	180	171	152	140	137	103
Guide Included (Section B-B of Fig. 12)	1	109	81	54	32	26	82	75	61	52	49	72	69	63	59	58	83
	0.7233	220	195	140	110	102	186	175	150	136	131	169	164	154	148	146	118

NOTES: Feed support = $\alpha = 0.22$, $\epsilon_{ext} = 0.24$, $\epsilon_{int} = 0.9$
Guide: $\epsilon_{ext} = \epsilon_{int} = 0.9$
Bellows: $\epsilon_{ext} = \epsilon_{int} = 0.8$
$K_{Invar} = 73.2$ BTU-in./hr-ft^2-^{O}F
$K_{bellows}$ is negligible
*See Figure 12, Configuration 1.

Table IV. Antenna Feed Temperatures

α	ϵ_{ext}	Astronomical Units	Node Number Temp (^{O}F)*					$T_1 - T_5$ (^{O}F)
			T_1	T_2	T_3	T_4	T_5	
0.22	0.24	1	64.04	63.98	63.84	63.75	63.72	0.32
		0.7233	156.30	156.18	155.92	155.75	155.69	0.61

NOTES: $K_{aluminum} = 1200$ BTU-in./hr-ft^2-^{O}F
*See Figure 12, Configuration 2.

assumed may raise or lower the indicated temperatures, but will probably have an adverse effect on thermal distortions. The antenna feed temperature data is shown to the second decimal place to indicate temperature differentials of less than one ^{O}F. The absolute temperature accuracy is several ^{O}F. Internal radiation for this configuration is relatively unimportant, so that the absence of black paint on the internal surface will not appreciably affect temperature differentials.

F. WEIGHT ANALYSIS

The JPL spacecraft antenna weight is given in Table V. Component weights shown in the "estimated" column were based on preliminary design layouts. Component weights shown in the "calculated" column were determined from production drawings. The actual weights were determined by weighing the various assemblies indicated in the "actual" column.

G. FABRICATION STUDY

The fabrication of the high-gain spacecraft antenna is unique in that it involves extremely thin gauge tubing and sheet stock of Invar and a Raschel lace screen of 3-mil Invar wire. Some minor problems were encountered in welding Invar to Invar, but with experience, these difficulties were overcome. Riveting presented no problems except accessibility for bucking the rivets.

Tubing (0.007-inch wall x 1-inch OD) was formed to the contour of the paraboloid. The tubing was filled with Cerebend before the forming process to prevent wrinkles or kinks. After forming, the Cerebend was melted out, a hinge bracket was welded to each tube, and each tube was partially filled with lightweight foam for structural integrity. The Raschel lace Invar wire screen was prestretched on a rig to ensure uniform screen rectangular apertures of approximately 1/8 x 1/4 inch (see Figure 13). The screen was then transferred to a frame (see Figure 14). Finally, the screen was placed on two adjoining ribs and attached to the ribs with epoxy (see Figure 15).

Table V. Weight Breakdown

ITEM	WEIGHT (POUNDS) ESTIMATED	CALCULATED	ACTUAL
Hub Structure	(7.530)	(6.778)	
Rim	2.056	1.906	
Reinforcing Ring	1.276	1.361	
Center Channels	0.998	0.812	
Ribs	1.606	1.292	
Center Plates	0.442	0.487	
Cross Members	0.196	0.268	
Diagonals	0.560	0.219	
Gussets and Weld	0.396	0.433	
Deployment Mechanism	(3.982)	(3.663)	
Sector	1.656	1.332	
Pulleys, Brackets, Guides and Hardware	1.128	0.771	
Drive Ring	0.598	0.668	
Cables and Fittings	0.468	0.688	
Locks and Stops	0.132	0.204	(22.18)
Reflector	(6.772)	(5.156)	
Ribs	5.748	4.044	
Surface	1.024	1.112	
Hinges	(5.188)	(4.613)	
Hinge Fitting Inboard	1.152	1.284	
Hinge Fitting Outboard	0.804	0.564	
Attachments	1.048	0.917	
Tube Support	0.888	0.660	
Hinge Pin	1.296	1.188	
Boom Support	(2.171)	(1.253)	
Guide Support	0.911	0.896	
Rollers, Brackets, and Hardware	1.260	0.357	
Boom	(2.949)	(5.726)	(5.20)
Truss	2.210	2.726	
Actuator	0.739	3.000	
Feed and Supports	(2.600)	(2.643)	(2.49)
Support Tubes	1.700	.825	
Feed Horn	.500	.500	
Fittings	.400	.780	
Actuation	--	.538	
Protective Canister	(2.250)	(1.671)	(2.10)
Totals	33.442	31.503	31.97

Unit aperture weight for antenna (total weight less canister and boom) $= \frac{23.42}{63.61} = 0.37$ psf.

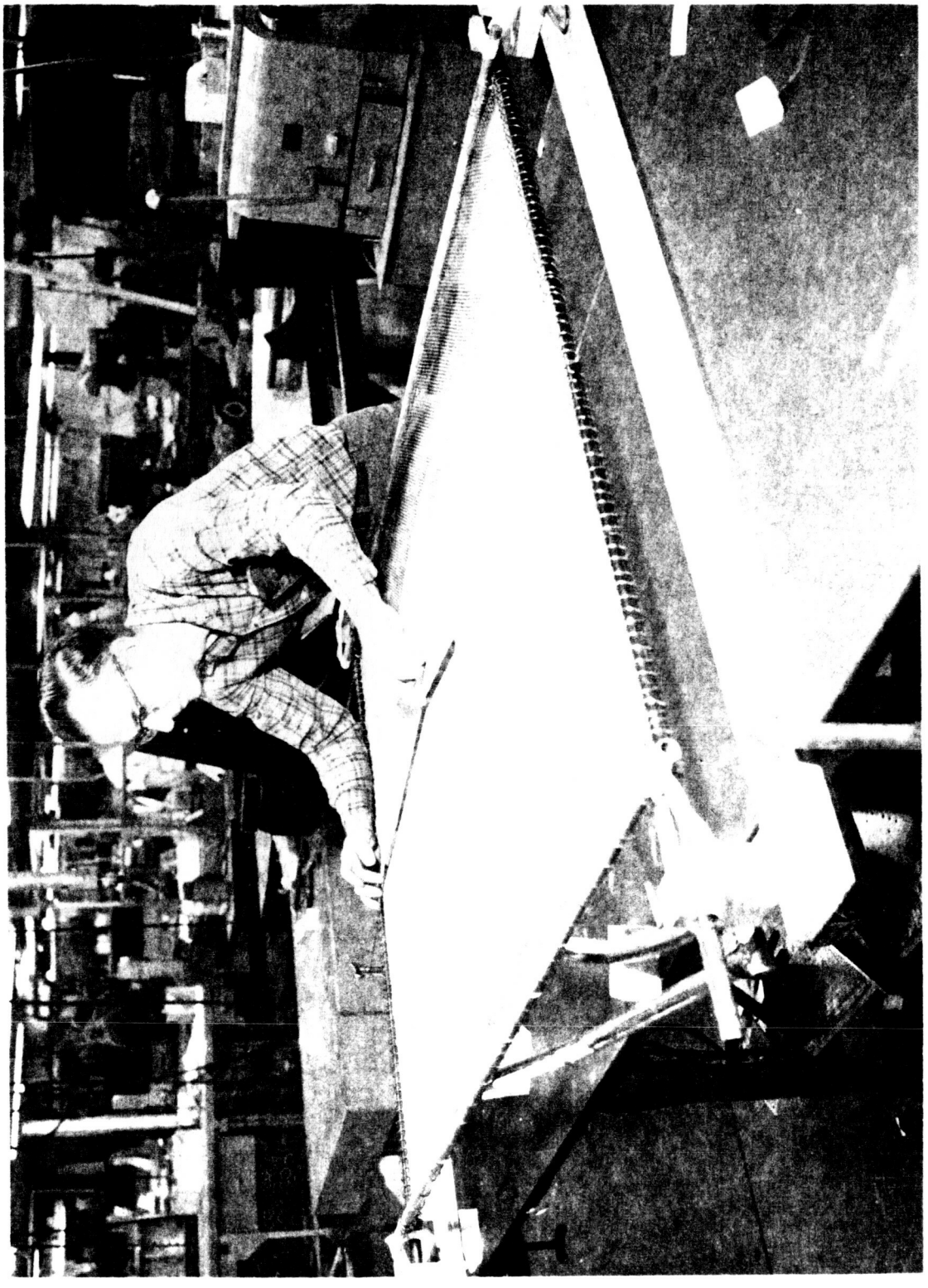

Figure 13. Prestretching Screen to Ensure Uniformity

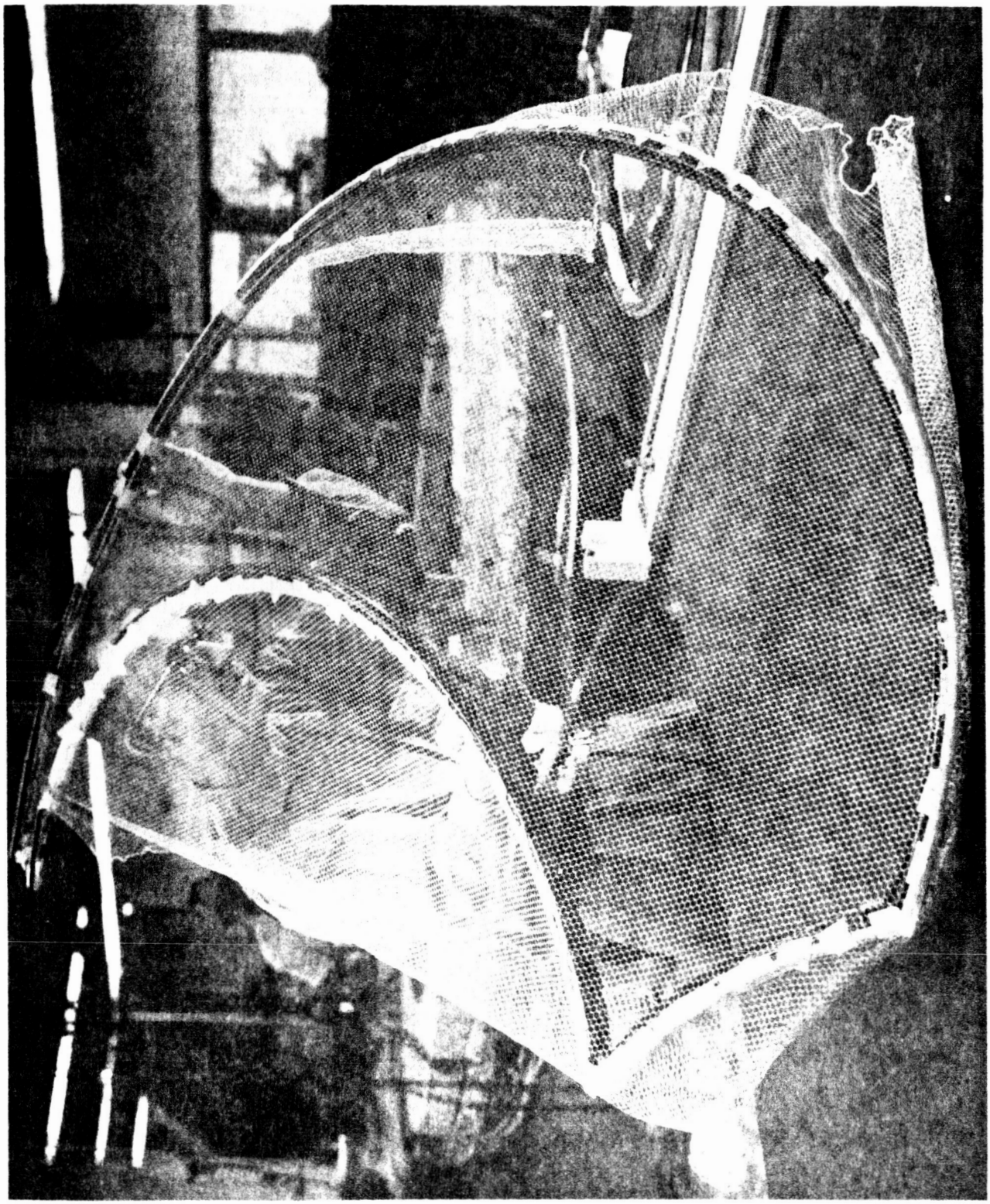

Figure 14. Forming Screen on Frame

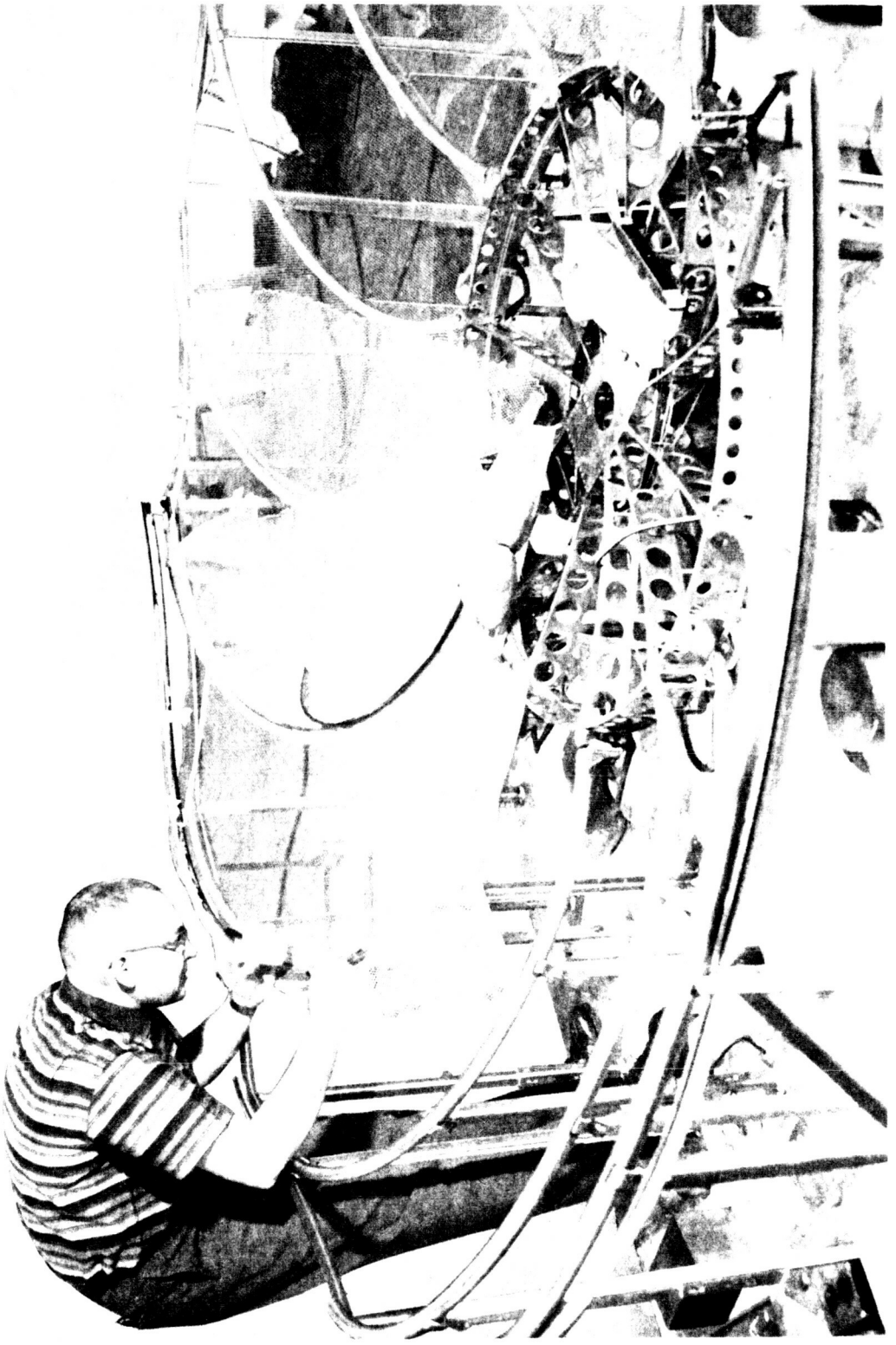

Figure 15. Attaching Screen to Adjoining Ribs

SECTION IV. MODEL TESTING

A. GENERAL

Test requirements outlined in JPL specifications included electrical, bell jar sample, contour, and vibration measurements.

This section describes the test procedure and presents results of each test.

B. ELECTRICAL

1. General

Electrical measurements were conducted using a dipole-disk feed to determine the gain of the antenna.

2. Test Equipment

The test range was 400 feet long; the transmitter and receiver stations were approximately 45 feet above the ground. The following transmitter station equipment was used:

(1) Signal generator

(2) Directional coupler

(3) Turret attenuator

(4) Transmit antenna (4-foot parabolic reflector)

(5) Frequency meter

(6) VSWR indicator

The following receiver station equipment was used:

(1) JPL high-gain antenna

(2) Dipole-disk feed (illumination pattern shown in Figure 16)

(3) Tuner

(4) Detector

(5) Recorder

(6) VSWR indicator

(7) Gain standard

3. Test Procedure

Prior to the initiation of this test, the receiver site was checked with a field probe. The antenna was installed and focus tests were conducted to determine optimum feed position. Measurements of gain were made by comparing the received signals of the antenna under test to the standard gain horn.

4. Test Results

The maximum gain measured on the test range was 32 db. This is 1.5 db down from a perfectly conducting solid surface containing a true paraboloidal shape (f/D = 0.35), which is 9-feet in diameter and scalloped at the periphery similar to the test antenna.

Independent calculations based on wave guide tests of the reflecting screen and contour measurements predicted a total loss of 1.66 db, which is 0.97 db reflector loss and 0.69 db loss due to fabrication tolerance. The variation between test results and calculations is well within test tolerances.

The screening material tested in a wave guide showed that 80 percent of the incident power would be reflected from this material in free space at 2295 mc.

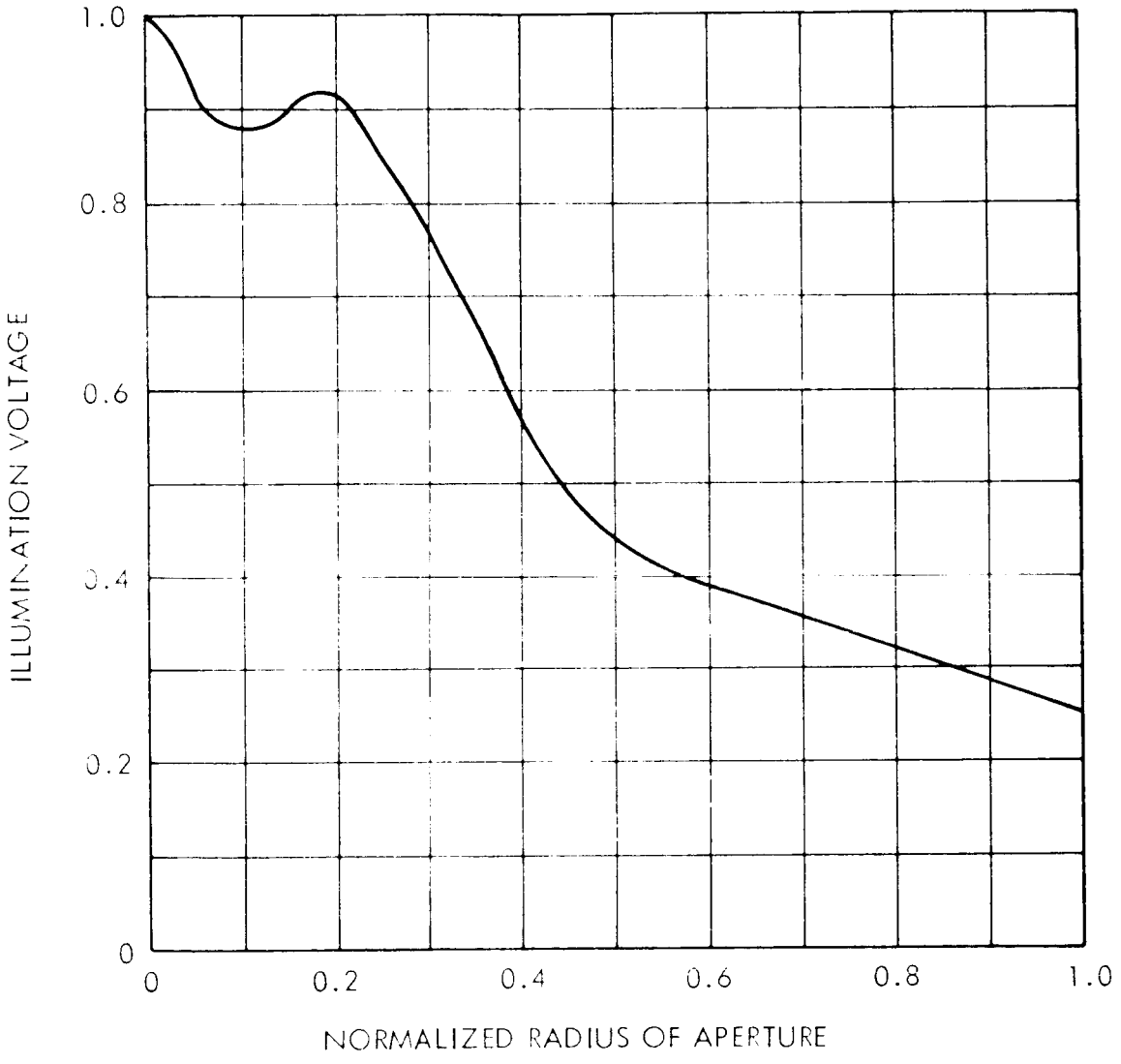

Figure 16. Average Pattern of E and H Planes of Dipole-Disk Feed

The 80 percent reflected power represents a 0.97 db gain loss for the antenna.

The losses caused by fabrication tolerances are separated into losses due to the flat bays between ribs of the deployed section (~0.45 db), the random errors inherent in manufacturing and positioning of the ribs (~0.23 db) and the losses in the fixed center hub area (~0.01 db).

C. BELL JAR SAMPLE TESTING

1. General

Vacuum and temperature tests on a boom and roller assembly, deployment mechanism, screen sample, and welded joint determined suitability for space applications.

2. Test Procedure

All components were subjected to the same vacuum and temperature exposure in a "CVC" oil diffusion pumped bell jar facility. Pressure was maintained at 5 to 10×10^{-6} mm Hg. The temperature on each component was reduced to $-10^{\circ}C$ and held for four hours, then raised to $75^{\circ}C$ and held for 12 days.

Test temperatures were obtained by a combination of an outer cold wall and inner wall heated by infrared lamps. Temperature was monitored and controlled through thermocouples welded to component areas considered most critical. Figure 17 shows the test setup for the boom and roller assembly. The force required to elevate the boom was measured before the test and at the end of each period of temperature exposure.

The test setup of the deployment mechanism is shown in Figure 18. The force required to operate the mechanism through 90 degrees was measured before the test and at the end of each period of temperature exposure.

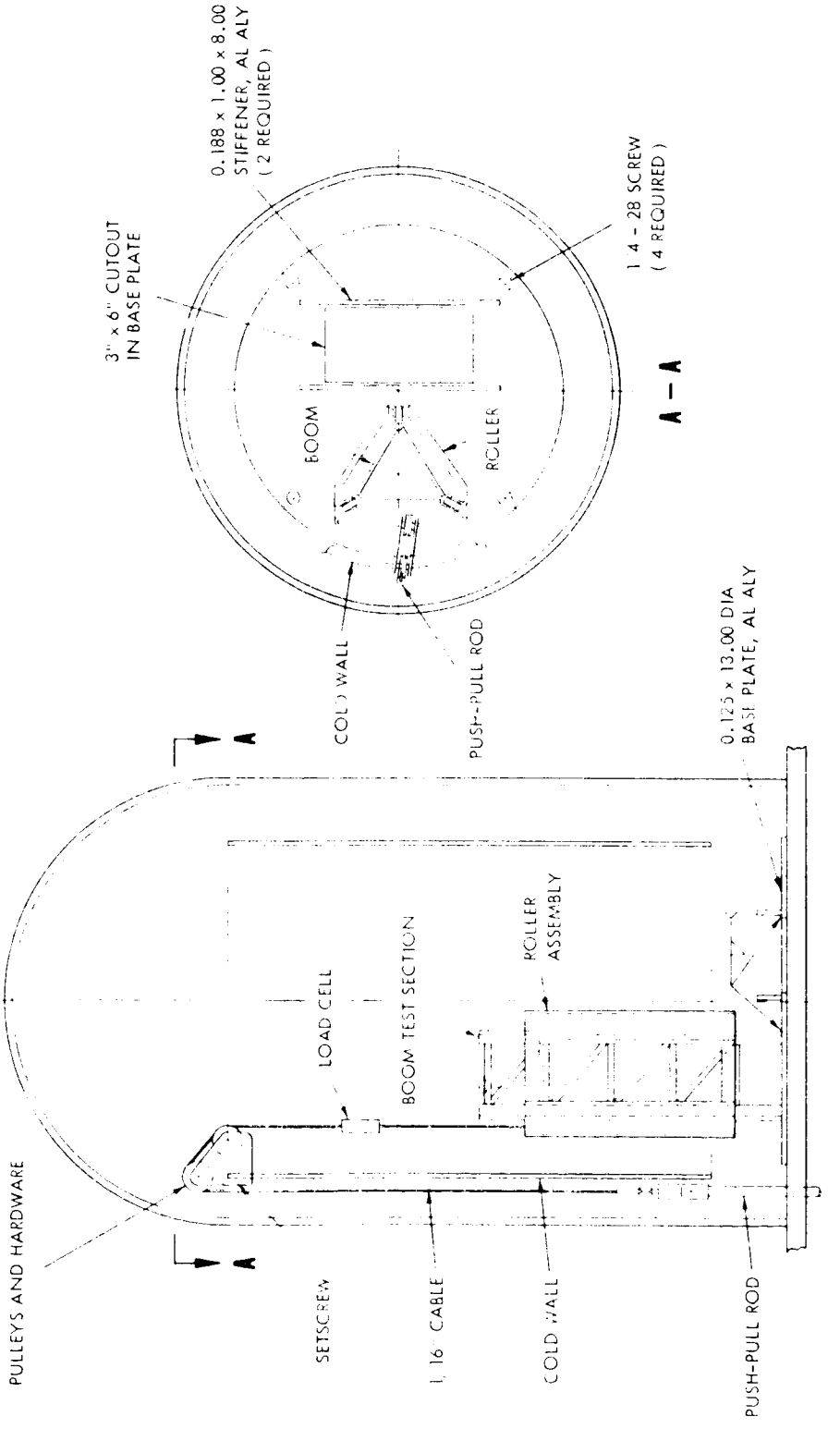

Figure 17. Boom and Roller Bell Jar Test

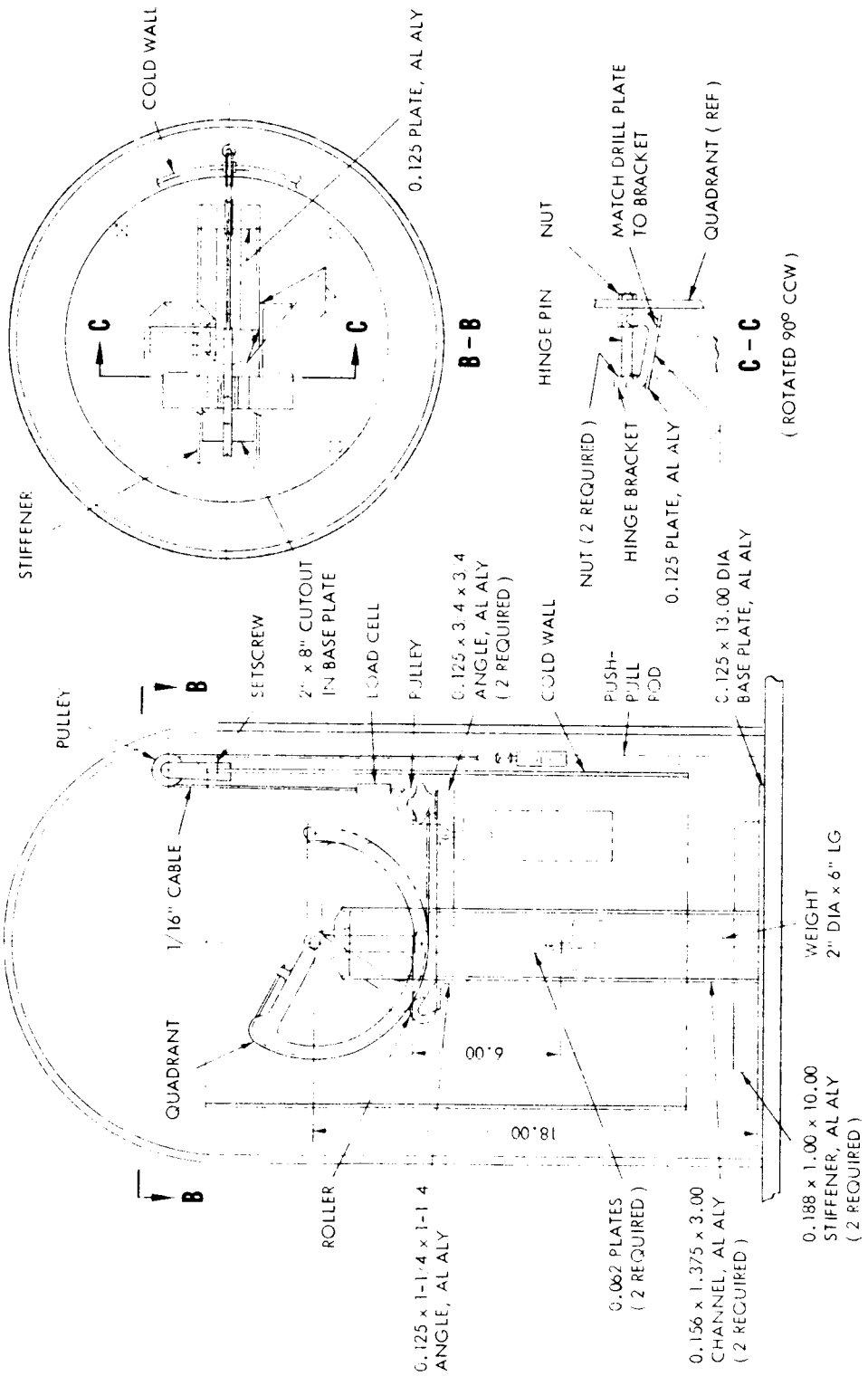

Figure 18. Deployment Mechanism Bell Jar Test

Screen samples and weld joints were tested in a bell jar, using a setup similar to Figure 17. Screen samples were visually inspected and flexed at the end of each period of temperature exposure to evaluate degradation of the screen-to-tubing bond. The welded joint was visually inspected for cracks or other surface degradation at the end of each temperature exposure.

3. Results

The only effect of exposure on the components was a slight binding of the boom assembly at 75°C, caused by thermal expansion of the system. This was not considered serious. Rollers remained free on their shafts, although indications were that most of the lubricant had been vaporized. To elevate the boom 3.25 inches at 21°C, an average force of 1.2 pounds was required, at -10°C an average of 1.05 pounds was required, and at 75°C an average of 2.2 pounds was required.

The deployment mechanism operated smoothly and consistently throughout the test with a load of 0.6 to 5.7 pounds.

No apparent degradation to the screen or bonding resulted from vacuum and temperature exposure.

No apparent degradation to the welded joint resulted from vacuum and temperature exposure.

D. CONTOUR TESTING

All contoured structural members and curved radial ribs were constructed, fitted, and assembled on a single male form block that defined the design specification paraboloid of revolution. Figure 19 shows the antenna under construction on the male form. The antenna reflector assembly without the screen was removed from the male form and checked for dimensional deviation under a 1-g influence with the parabolic surface vertically up and vertically down. Dimensional deviation was determined as shown in Figure 20, and then contour adjustments were

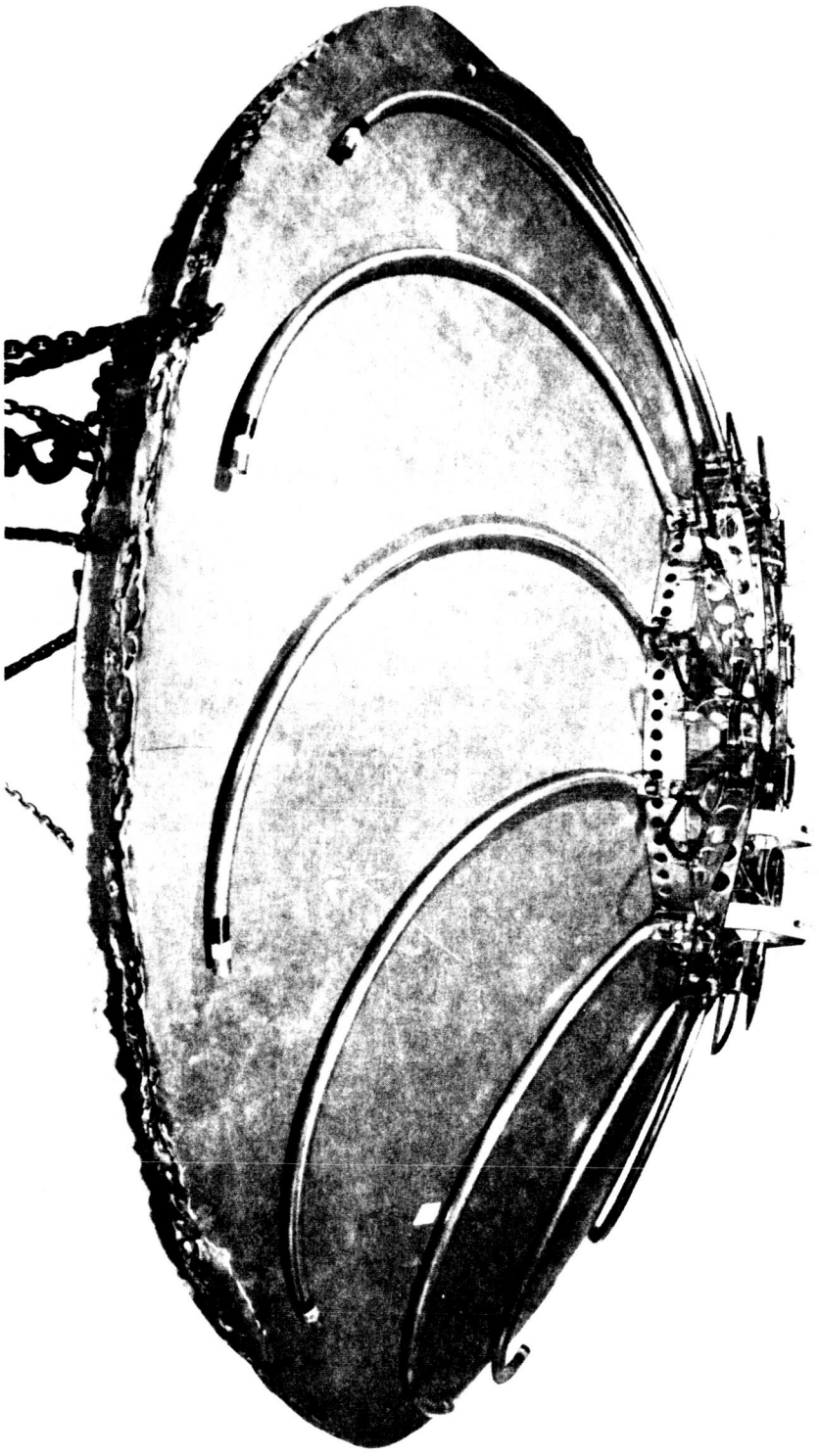

Figure 19. Antenna under Construction on Male Mold

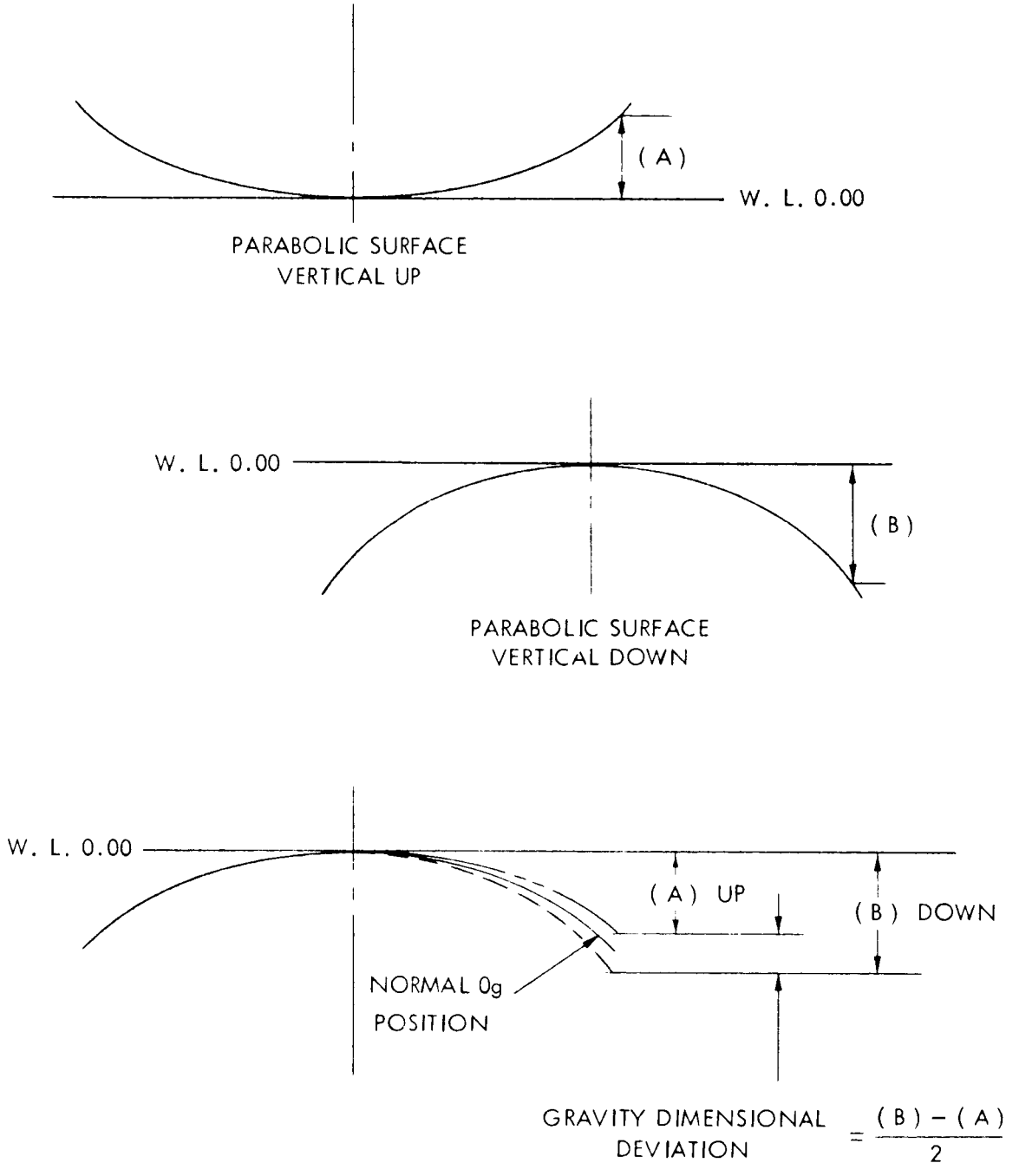

Figure 20. Determining Dimensional Deviation of Contour under 1-g Influence

made at the hinges of the curved radial ribs. The hinges provide the only means of contour adjustment. The adjusted reflector was placed in a fixture, and Raschel lace-styled Invar wire screen was applied (see Figure 15) to complete the reflector.

When the reflector was removed from the fixture, dimensional deviations were again determined and again adjustments were made as necessary. The contour was checked at the 32-, 43-, and 53-inch radii on the paraboloid surface of each of the 12 curved radial ribs and the screen between the ribs.

The following tolerances were measured:

	± 1-g Load	Normalized 0-g Load
Maximum Deviation	±0.61 inch	±0.43 inch
Maximum Deviation with Optimum Positioning	±0.40 inch	±0.31 inch

E. VIBRATION TESTS

1. Test Description

To determine antenna structural characteristics, the unit was vibrated in three mutually perpendicular axes in both the packaged and deployed configurations as shown in Figures 21 and 22.

The antenna was mounted on an MB C-25 vibration exciter (MB Electronics Corp. New Haven, Conn.). Gulton accelerometers were used at pickup points for monitoring.

The frequency range for the tests was between the limits of 10 to 1500 cps. Variable loading ranged from 0.3 to 3 g's. Vibration axis and pickup locations for the packaged configuration are shown in Figures 23, 24, and 25. The vibration axis and pickup locations for the deployed configuration are not shown in detail because of relatively low response.

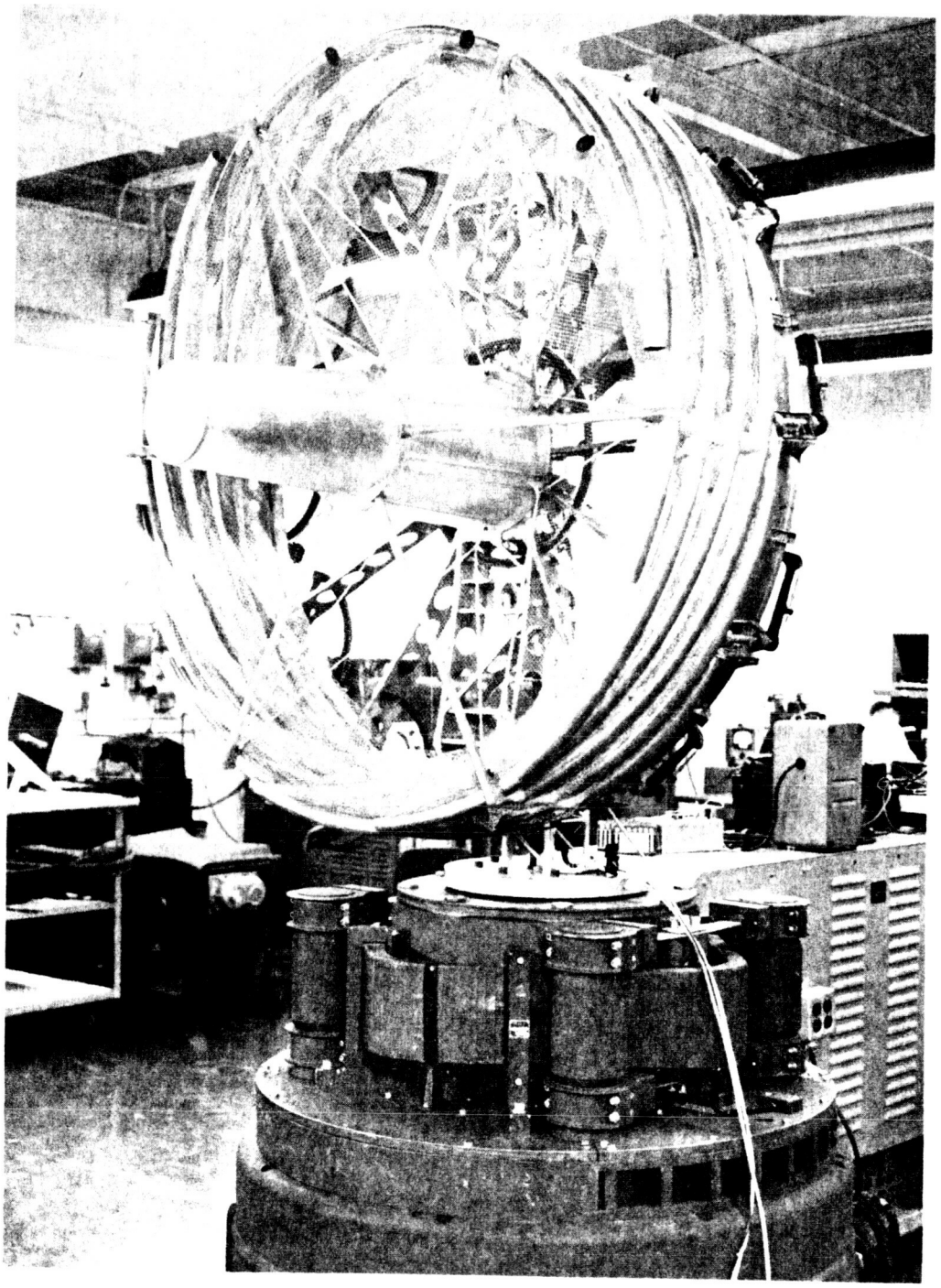

Figure 21. Vibration Testing Antenna in Packaged Configuration

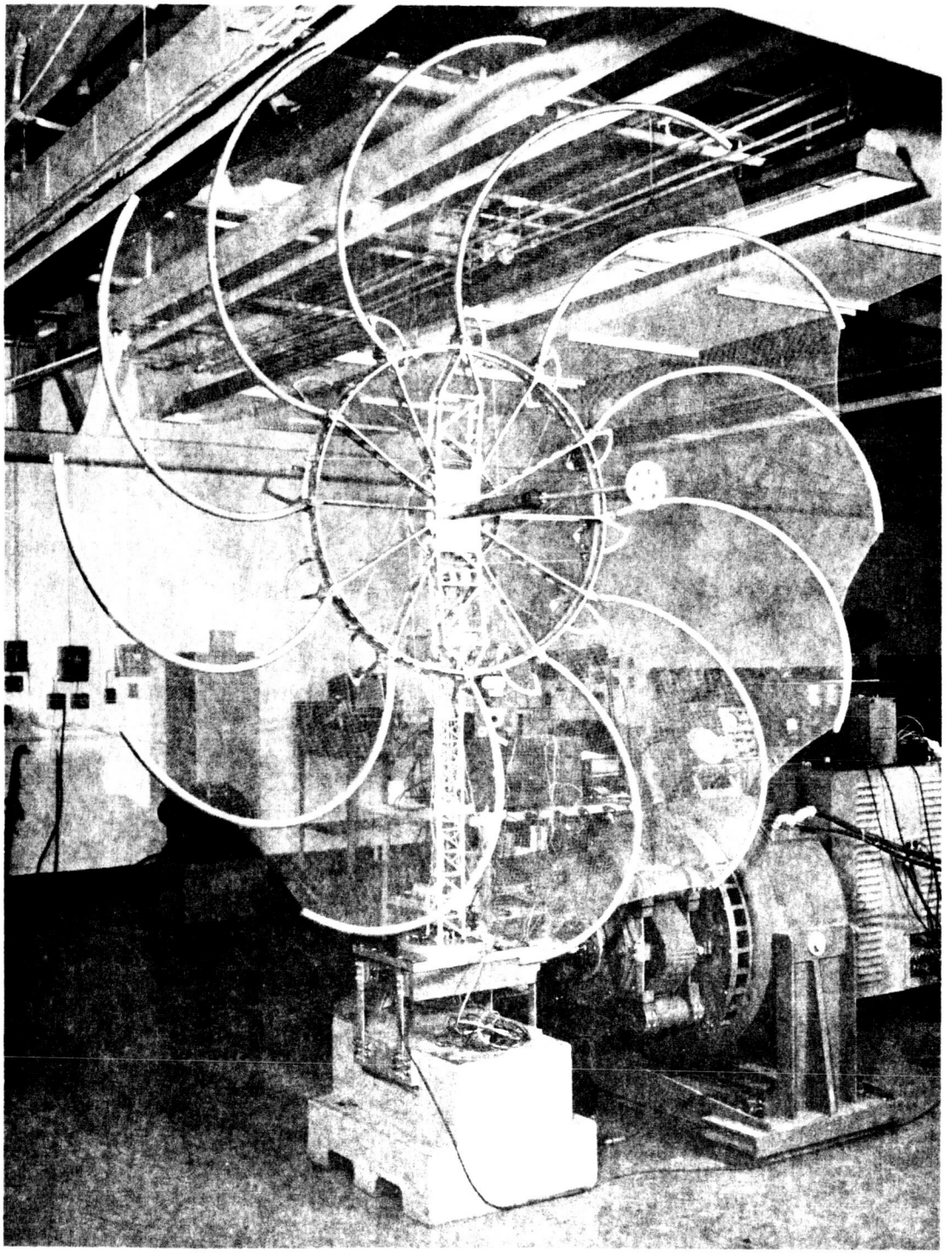

Figure 22. Vibration Testing Antenna in Deployed Configuration

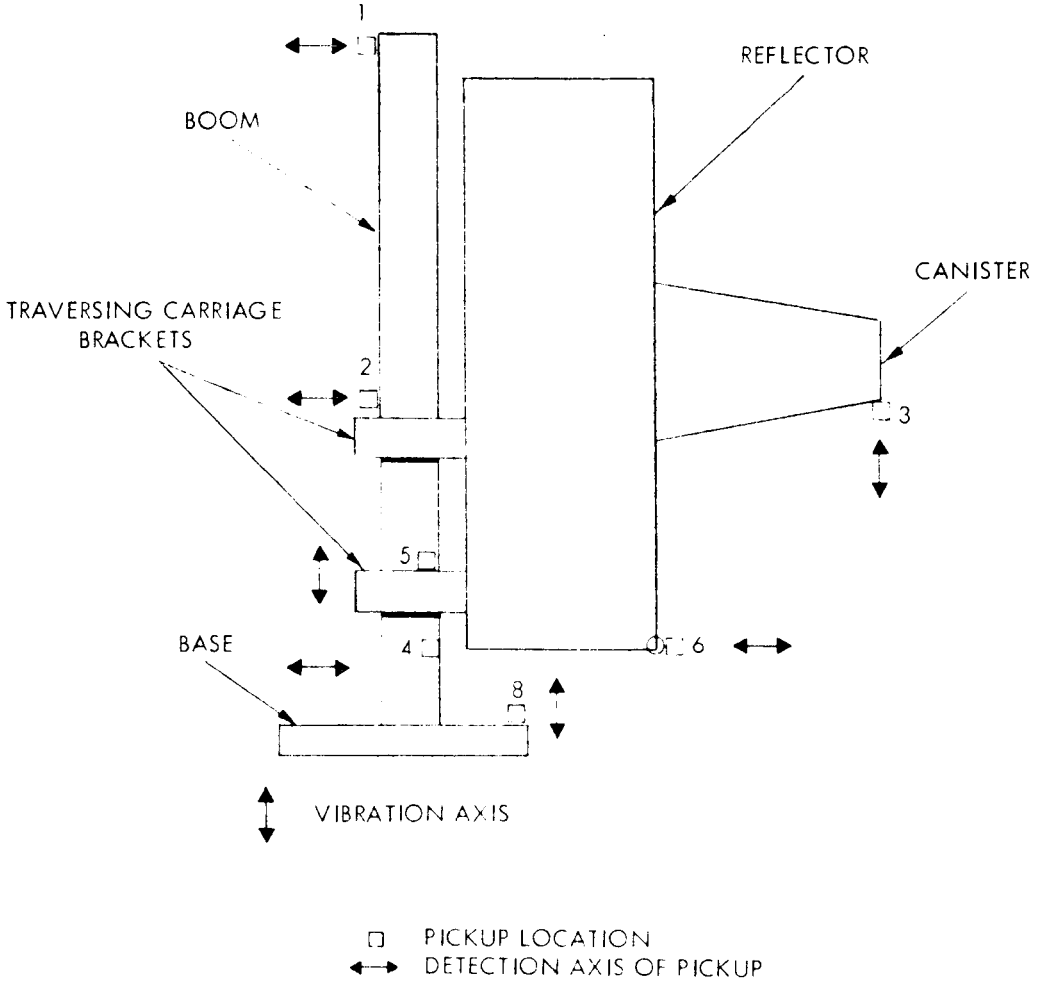

PICKUP LOCATION

1. Top of Boom Structure
2. Middle of Boom Structure
3. End of Canister
4. Lower Boom Structure
5. Lower Boom Bracket (Vertical Axis)
6. Extremity of Curved Radial Tube
7. Not Used
8. Base

Figure 23. Vibration Test Axis 1 (Packaged)

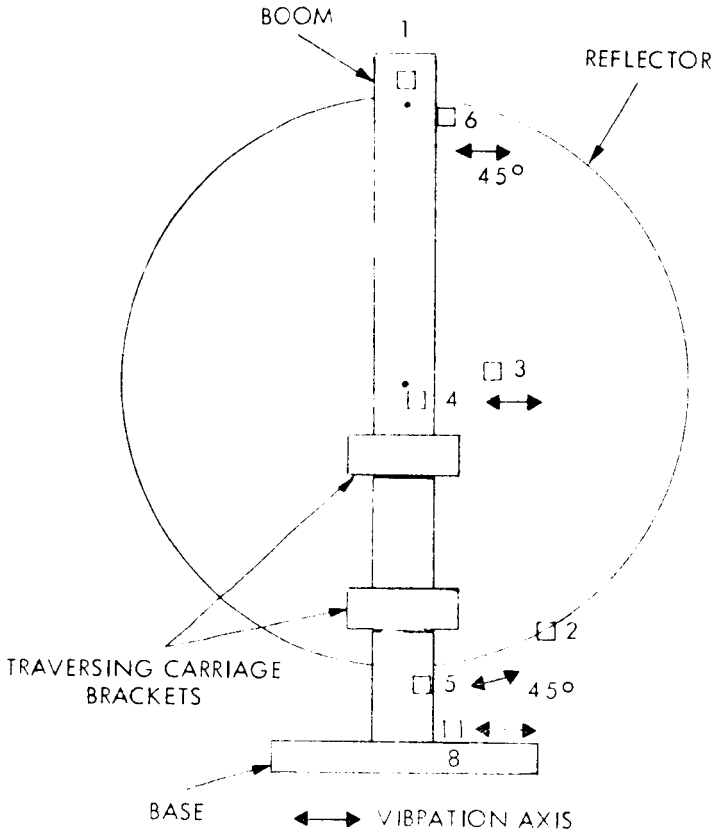

□ PICKUP LOCATION
↔ DETECTION AXIS OF PICKUP
● DETECTION AXIS OF PICKUP IN PERPENDICULAR PLANE

PICKUP LOCATION

1. Top of Triangular Boom Structure
2. End of Curved Radial Tube
3. Canister
4. Lower Half of Triangular Boom Structure
5. Right Side of Triangular Boom Structure - 135° Lower End
6. Right Side of Triangular Boom Structure - 45° Upper End
7. Not Used
8. On Mounting Plate

Figure 24. Vibration Test Axis 2 (Packaged)

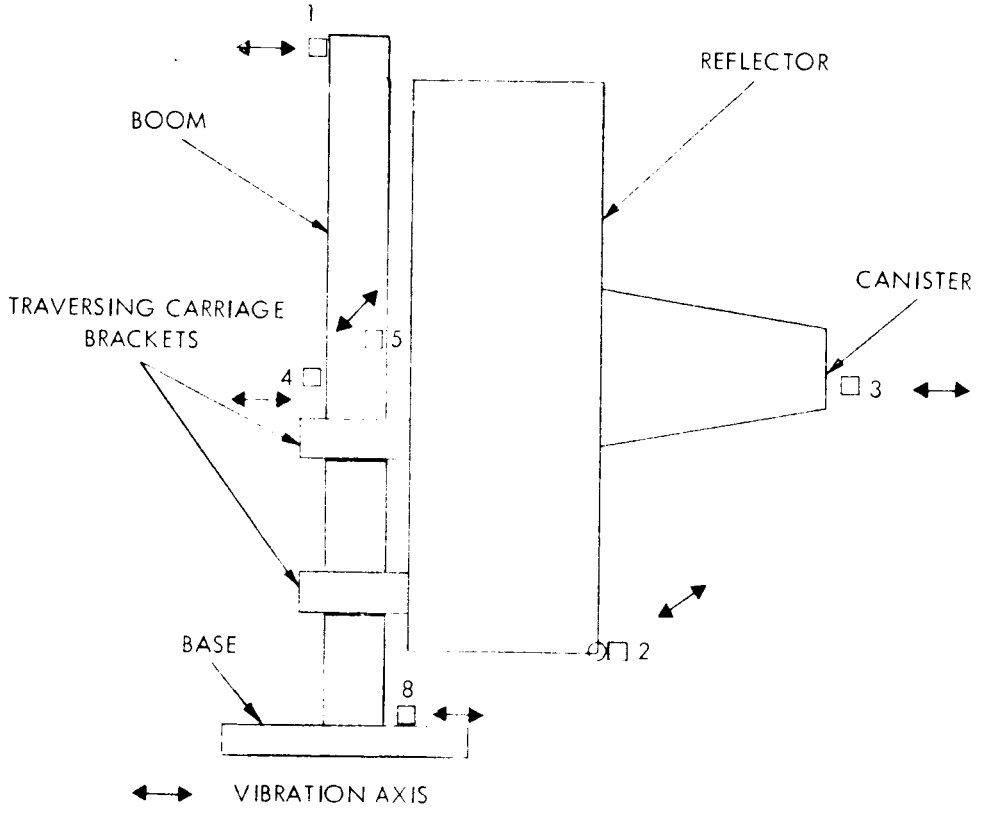

PICKUP LOCATION

1. Top of Boom
2. End of Curved Radial Tube
3. End of Canister
4. Middle of Boom
5. Mast Middle of Boom 45° to Vibration
6. Not Used
7. Not Used
8. Base

Figure 25. Vibration Test Axis 3 (Packaged)

2. Deployed Vibration Tests

In the deployed condition, very little response was noted. For axis No. 2, a mild response was noted at 35 cps. The amplification factors were 4.5 on the feed, 6 on the top of the boom, and 14 on the end of the tube. The mode was primarily that of the reflector rotating about the center line of the boom, with the boom serving the function of the spring. This response should not be a source of concern because the inputs are small when the screen is deployed. Along axes No. 1 and 3, noticeable response was discerned.

3. Packaged Vibration Tests

a. Axis 2 (see Figure 24). Along axis No. 2, two natural frequencies are noted. Both frequencies have amplification factors of 40 with a 0.3-g input and about 20 with a 3-g input. The lower frequency occurs at 13 cps and seems to be boom bending with a large rotary inertia on its end. This mode can be eliminated by furnishing a support at the top of the triangular boom. This support would be a part of the missile structure. The higher mode occurs at 30 cps and is a coupled mode consisting of boom bending combined with boom torsion. The amplitude of this mode would also be decreased by supporting the tip of the boom. If the packaged screen could be lightly stabilized at the extremities of the outer wall of the tubes so as to resist torsion in the boom due to rotation of the packaged mass about the boom axis, the amplitude of this motion can be markedly decreased. During the test, the motion was restrained with slight pressure of the finger tips.

The dynamic loads measured at the top of the boom during the 3-g input were 60g's. It is felt that these high loads caused the failure that occurred when a 3-g input was applied along axis No. 1 in the subsequent shake.

b. Axis No. 1 (see Figure 23). The structure failed during this portion of the test. The sequence of testing under 3-g input was axes 3, 2, and 1.

The resonance frequency that caused failure was at 13 cps, which is the boom bending mode. Since the cg of the packaged antenna is so eccentric to the center line of the truss, this mode is easy to excite when shaking along the long axis of the boom. A support from the missile skin to the top of the boom will reduce the amplitude of this mode.

c. Axis No. 3 (see Figure 25). When fiberglass cord was used for packaging, resonances (f) and amplification factors (Q) were noted as follows:

Pickup No.	1	2	3	4	5	8
f	13	40	60	63	90	130
Q	25	9	13	10	8	6

When the fiberglass cord was replaced with wire and the tube ends were stabilized with polystyrene blocks, no detectable response was noted with the same input as used previously.

Examination of the vibration traces showed excessive hammering at the points where the two pins lock the movable packaged reflector to the boom. This condition could be improved considerably by utilizing tapered pins and a cushion of soft rubber or elastomer between the mating faces.

4. Vibration Test Summary

A summary of the results of the engineering vibration testing is as follows:

(1) Stabilizing the top of the boom structure attached to the spacecraft during launch would considerably reduce dynamic response.

(2) Light pressure on the periphery of the packaged antenna is desirable if practical, but not as imperative as stabilizing the boom.

(3) Use of wire instead of fiberglass cord and use of polystyrene blocks lessened response.

(4) A cushion of flexible rubber with tapered pins is essential to prevent hammering.

SECTION V. GROUND DEPLOYMENT OPERATING INSTRUCTIONS

A. GENERAL

The operating instructions for ground deployment of the spacecraft antenna are given in this section. The three basic procedures are (1) preparation for deployment, (2) deployment, and (3) returning the antenna to the packaged configuration. It is assumed that operators are basically familiar with the equipment covered. The instructions are intended to serve as an outline only, with emphasis on procedures unique to the spacecraft antenna. Observe normal safety precautions, particularly in the handling of igniters. Refer to "Description" and "Antenna Deployment" subsections in Section III.

B. PREPARATION FOR DEPLOYMENT

Perform the following procedure to prepare the antenna for ground deployment (see Figures 26, 27, and 28).

(1) Mount the antenna assembly with the boom horizontal to the ground plane so that the feed will be facing upward after deployment, as shown in Figure 28.

> NOTE: The 1 x 12 inch diameter mounting plate (5, Figure 26) has clearance holes for 0.375-inch diameter bolts to facilitate the antenna mounting.

(2) Make certain that a 28 VDC, 10-ampere power source is available for deployment.

> NOTE: Antenna functions are individually performed only by direct connection to the power source; functions are not automatic.

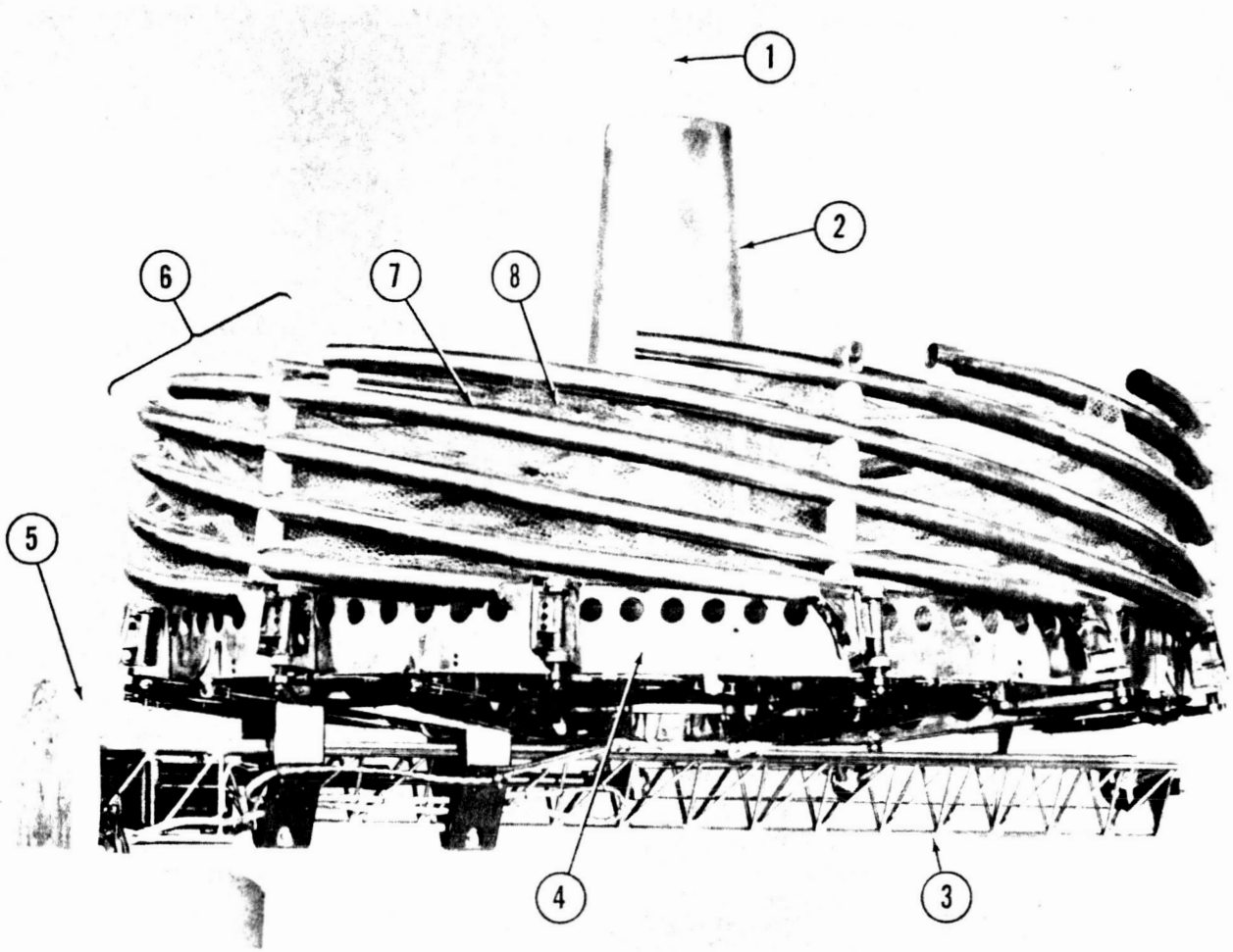

1. Cable
2. Canister
3. Deployment Boom
4. Hub
5. Mounting Plate
6. Reflector
7. Curved Radial Rib
8. Orthotropic Screen

Figure 26. Antenna in Packaged Configuration

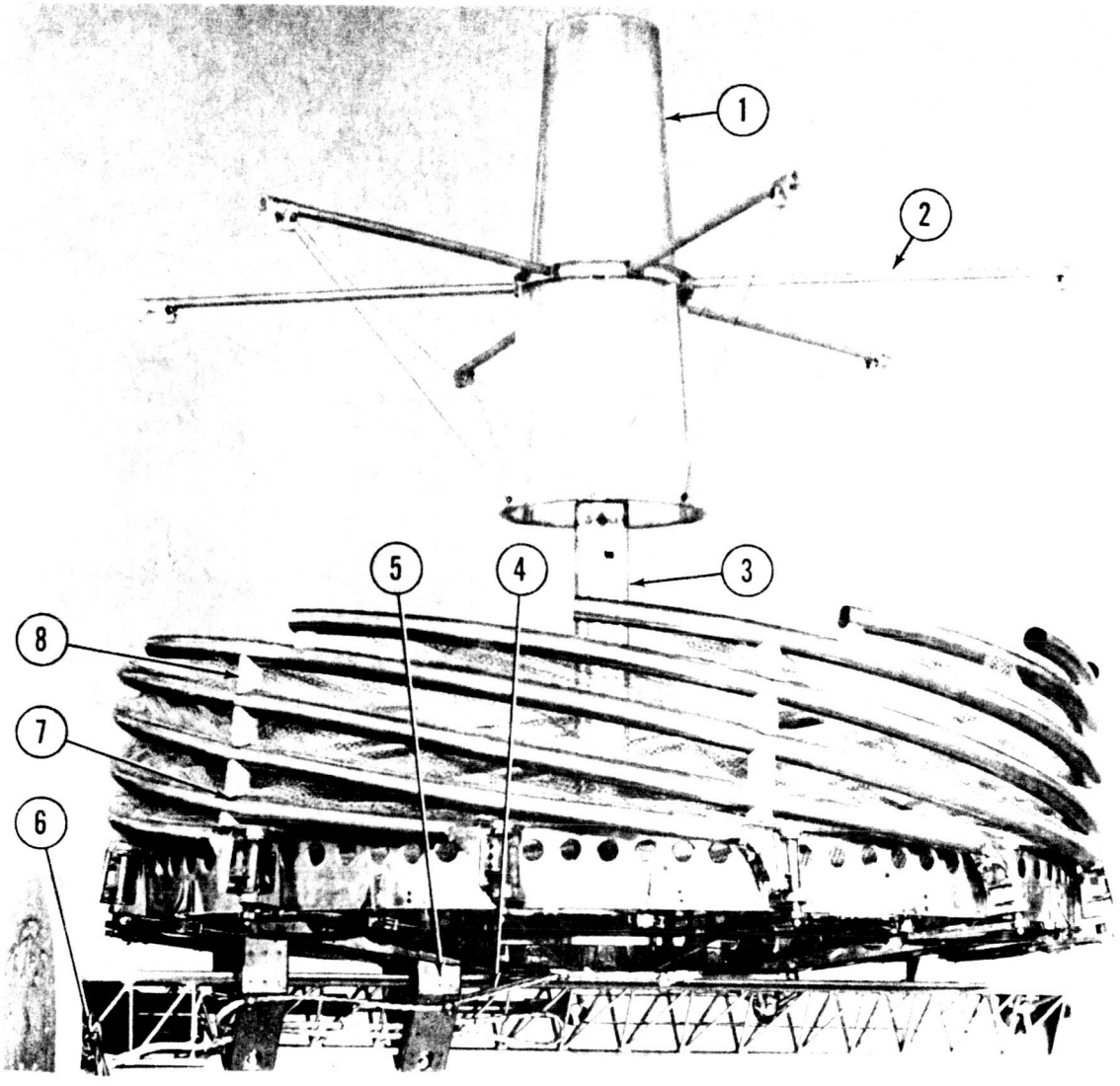

1. Canister
2. Canister Arm
3. Feed Support
4. Coaxial Cable
5. Spring Clip (under bracket, not shown)
6. Electrical Cable Assemblies
7. Chafe Pad (under Spacer Blocks)
8. Spacer Blocks

Figure 27. Antenna after Canister Separation

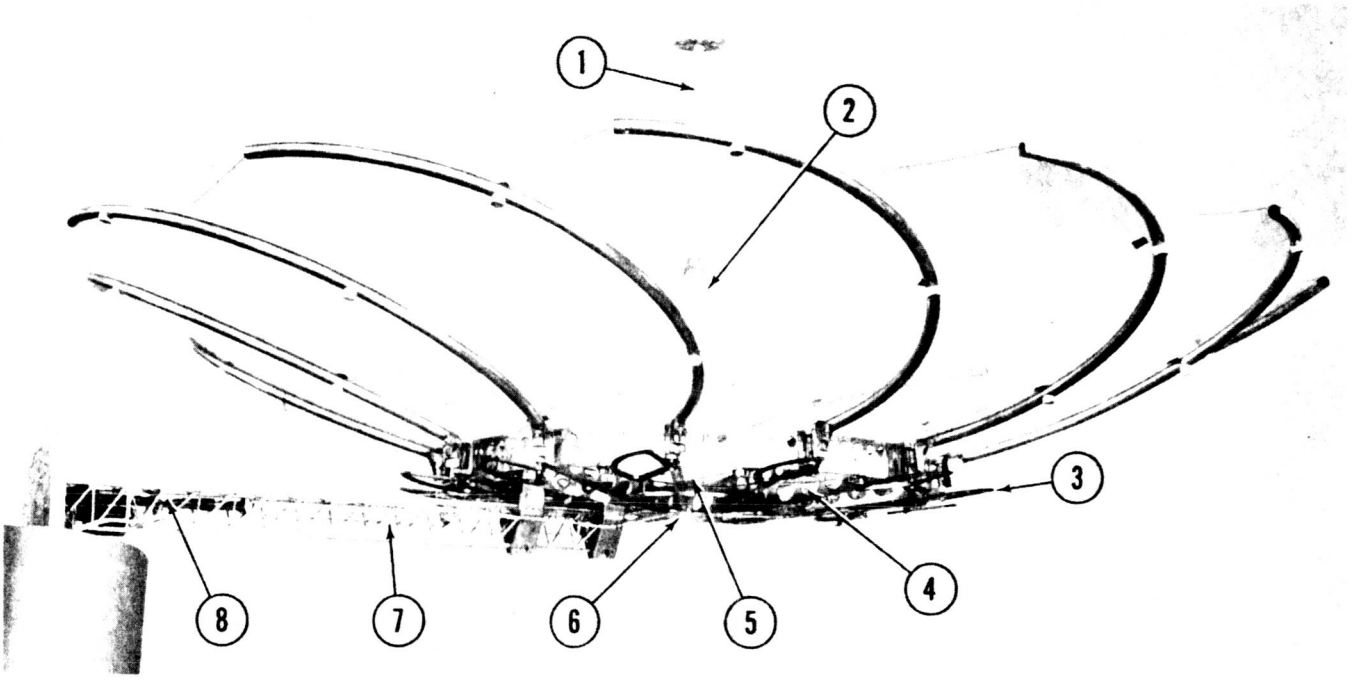

1. Feed
2. Feed Support
3. Deployment Quadrant (Typ)
4. Explosive Actuated Gas Energy Release
5. Pin Pusher (Typ)
6. Well Cover
7. Drive Cable
8. Ball Release (Typ)

Figure 28. Antenna Deployed

(3) Secure the cable (1, Figure 26) to the canister (2, Figure 26), and counterbalance the canister weight (approximately two pounds) over pulleys.

CAUTION

Make certain that the cable to the canister aligns with the center line of the feed (1, Figure 28).

(4) Splice a four-inch extension on the leads of the Mk 54, Mod 0 igniters* of the three 6071 pin pushers (5, Figure 28) and the two 6072 ball releases (8, Figure 28).

(5) Splice the pin pusher igniter extensions to the respective circuit wiring labelled "CANISTER SEPARATION SQUIB LEAD CONNECTION."

(6) Splice the ball release igniter extensions to the respective circuit wiring labelled "ANTENNA BOOM SEPARATION SQUIB LEAD CONNECTION."

(7) Solder squib leads from the explosive actuated gas energy release**(4, Figure 28) to FEED EXTENSION SQUIB LEAD terminals (refer to Table VI) on terminal block of mounting plate (5, Figure 26).

C. DEPLOYMENT

To deploy the antenna from the packaged configuration, perform the following procedure (see Figures 26, 27, and 28).

NOTE: Deployment includes (1) canister separation, (2) feed extension, (3) antenna-boom separation, and (4) antenna deployment.

*McCormick-Selph Associates, Hollister, California.
**Eager Pak, Conax Corporation, Buffalo, New York.

Table VI. Mounting Plate Terminal Block Terminal Identification

TERMINAL NO.	IDENTIFICATION
1 and 2	Feed extension squib leads
3 and 4	Canister separation squib lead terminals
5	Antenna actuator common
6	Antenna actuator forward
7	Antenna actuator reverse
8 and 9	Antenna boom separation squib lead terminals
10	Shield tie

CAUTION

The four dc power cable assemblies supplied are tagged according to deployment function and should be used in the order specified. The canister separation power cable, feed extension power cable, and antenna-boom separation power cable are supplied with alligator-type clips. The red collared clip is the positive (+) lead, the braided bare wire attached to the black clip is the ground lead, and the third clip is the negative lead. The two bare ends of the fourth cable assembly are tagged "ANTENNA ACTUATOR POWER +TERMINAL and ANTENNA ACTUATOR POWER -TERMINAL."

(1) Connect the canister separation power cable to the 28 VDC, 10-ampere power source to effect canister separation.

NOTE: Counterbalancing of canister weight will prevent the canister from falling to the antenna surface after separation.

(2) Disconnect the canister separation power cable from the power source.

(3) Connect the feed extension power cable to the 28 VDC, 10-ampere power source to effect extension of the feed.

(4) Disconnect the feed extension power cable from the power source.

(5) Connect the antenna-boom separation power cable to 28 VDC, 10-ampere power source to effect antenna-boom separation.

(6) Disconnect the antenna-boom separation power cable from the power source.

(7) Connect positive and negative antenna actuator power leads to the 28 VDC, 10-ampere power source.

(8) Move the switch on the antenna actuator box from the center-off position to FWD and hold until the actuator is fully extended.

NOTE: The internal limit switch controls extension travel.

D. RETURNING ANTENNA TO PACKAGED CONFIGURATION

Perform the following procedure to return the antenna to the packaged configuration (see Figures 26, 27, and 28).

NOTE: The parts required to prepare antenna for reuse (O-rings, shear pins, etc) are supplied with the antenna.

(1) Remove the three pin pushers (5, Figure 28) and the two ball releases (8, Figure 28).

(2) Prepare the pin pushers and ball releases for reuse as follows:

(a) Disassemble each unit.

(b) Clean gas chamber. Replace O-rings as required.

(c) Reassemble.

NOTE: Install new shear pins in the pin pushers.

(d) Install the pin pushers and ball releases in respective locations.

(e) Retract the plunger of the ball release until the balls are flush with the housing barrel.

(3) Retract the feed (1, Figure 28) as follows:

(a) Remove the four screws and washers from the well cover (6, Figure 28) on the bottom of the antenna in line with the feed; then reinstall the screws as retainers for the gasket and well.

(b) Remove the eight additional screws that do not have washers, and remove the well cover.

(c) Install a support under the boom (3, Figure 26) near the end.

(d) Gently push the feed (1, Figure 28) into the feed housing (2, Figure 28), guiding the feed and coaxial cable (4, Figure 27) through the bellows.

(e) When the feed is fully retracted, coil the coaxial cable in the well.

(f) Replace the cover.

(4) Lift the spring clips (5, Figure 27) on the antenna end of the boom, and move the antenna away from the boom.

(5) Manually maintain a constant tension on the drive cable (7, Figure 28), and hold the antenna actuator switch in REV until the actuator is fully retracted (antenna engages ball releases).

NOTE: Manual tension may be relieved when slack is taken up in the drive cable.

CAUTION

During actuator retraction, the antenna radial contoured ribs will move toward the antenna hub. Make certain that the radial contoured ribs do not snag the antenna reflector screen.

(6) Push the plungers of the ball releases until the antenna is in locked position; then install the ball release shear pins.

(7) Make certain that the radial contoured ribs are fully nested around the antenna; then insert the spacer blocks (8, Figure 27) so that a fold of the intermediate reflector screen is nested between the rib and spacer block and extends away from the feed.

CAUTION

The spacer blocks are matched sets. Make certain that the numbers on the spacer blocks match the numbers on the radial contoured ribs.

(8) Place the 1 x 1 inch rubber chafe pad (7, Figure 27) inside the fold of the screen.

(9) Apply masking tape adjacent to the spacer blocks to hold the spacer blocks in position.

(10) Position the canister (1, Figure 27) so that the numbers on the canister arms (2, Figure 27) match the numbers on the top spacer blocks.

(11) Push the canister down on the feed housing, engage the pin pushers, and install nuts to hold the canister in position.

(12) Apply breakaway ties to antenna deployment quadrants (3, Figure 28), drive cable (7, Figure 28), and electrical cable assemblies (6, Figure 27).

NOTE: Use No. 8 thread for quadrant and drive cable ties. Use No. 24 thread for electrical cable assemblies.

SECTION VI. CONCLUSIONS AND RECOMMENDATIONS

The advanced development model of the high-gain spacecraft antenna proved the practicality of using large deployable antennas for planetary mission spacecraft. Although all antenna characteristics were not optimized during this program, the following were either developed or proven on this 9-foot diameter model:

(1) A deployment concept suitable for either 1 g or 0 g.

(2) The fabrication technique using Invar as a structural material.

(3) A weaving technique for reflective material which has orthotropic characteristics.

(4) Deployed packaged ratio of 2.4.

(5) Unit weight of 0.37 psf of aperture for a deployable antenna and feed.

(6) Gain of at least 32 db for a 9-foot diameter deployable antenna.

Other deployment schemes were established during the program, and their relative merit and feasibility were investigated. The primary consideration was to increase the packaging ratio to at least 9 with deployed diameters to 35 feet. The results of this study are presented in Table I.

The favorable results of the existing program indicate the desirability of continuing work to optimize the configuration. The proposed program of studies and fabrication of an advanced engineering model would include the following:

(1) Reduction of the surface tolerance to at least ±0.20 inch for zero gravity condition.

(2) Reduction of the rib tip deflections to at least ±0.10 inch for ±1-g loading.

(3) Increasing the screen reflectance to at least 96 percent.

(4) Installation of an operational feed.

(5) A reliability study.

(6) Weight reduction.

(7) Minimization of electrical blockage of the antenna hub in the packaged condition.

(8) Investigation of product improvement items such as rib supports, chaffing strips, breakaway cord ties, and sector locks.

APPENDIX A. ANTENNA ELECTRICAL CHARACTERISTICS

1. GENERAL

The effects of mechanical design parameters on the radiation characteristics of an antenna were investigated. Parameters considered were the number of rib sections, tolerance of the ribs, tolerances in the inner nonfoldable section, outside diameters, and illumination tapers. Primary consideration was given to the gain reduction caused by these parameters. The antenna is an unfurlable-type paraboloid consisting of a reflector whose outer sections are unfurlable. The curved ribs rotate into position, providing a singly covered surface between any two ribs (see Figure 1). Specification requirements for the antenna were the same as those imposed by JPL and detailed in Section I.

Only surface errors were considered for the study. The investigation required a study of surface deviations from a true paraboloid and their deleterious effect on gain and side lobes. More emphasis was placed on gain reduction than on side lobe performance.

2. SURFACE ERROR FUNCTIONS

Several sources of surface error exist in the subject of this study, reducing the aperture efficiency from that of an ideal paraboloid. Errors investigated are due to a single-curved surface between rib sections, manufacturing errors in the ribs, and surface errors in the center section. Actual departure from a true paraboloid in the outer skirt sections is a function of number of ribs, weave pattern of the screen, orientation of the screen weave pattern to the ribs, and screen material. In a preliminary study of contour error (Reference A-1), wire elements were assumed with each wire originating at some point on one rib, say

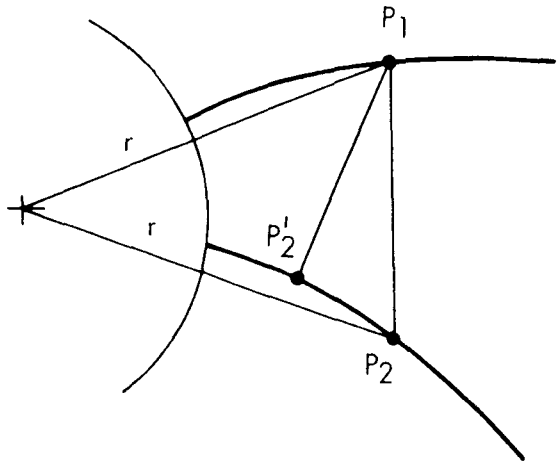

Figure A-1. Rib Geometry

P_1, extending to the nearest point on the adjacent rib, P_2' (see Figure A-1). To simplify the analysis, it might be assumed that a wire extending from P_1 to P_2 on the adjacent ribs is typical of the family of similarly placed wires making up the reflector surface. These two points, P_1 and P_2, are equidistant from the center. This approximation worsens as the radial distance increases. However, since the illumination decreases on the extremities, this approximation handicap is lessened.

Since this of type contour is assumed, the geometry of Figure A-1 may have the curved ribs replaced by radial ribs, and the geometry between the ribs remains the same. Considering this arrangement, as in Figure A-2, where a point (r, z) on the true paraboloid is rotated through the angle ζ and a similar trace $-\zeta$, a straight line drawn between these two points will have a maximum deviation from the true paraboloid at point (r', z').

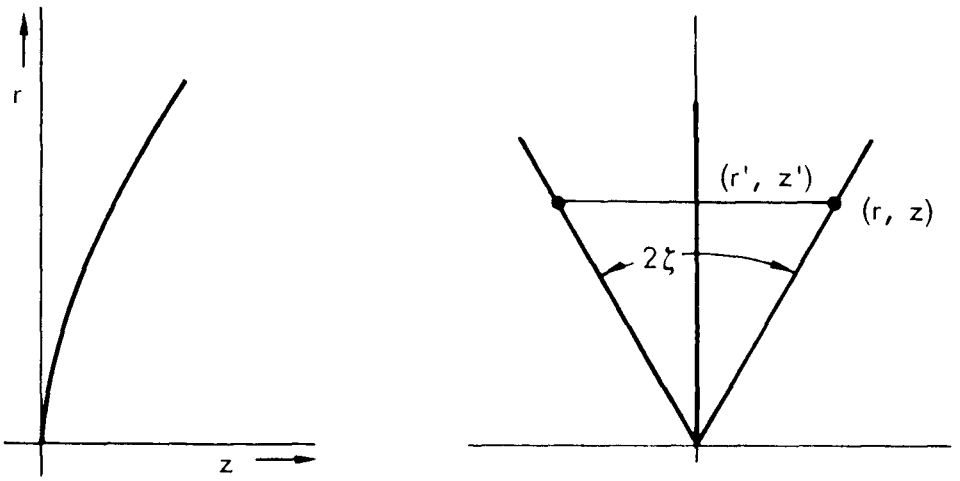

Figure A-2. Outer Skirt Error Geometry

These points are related by

$$z = \frac{r^2}{4F} \tag{A-1}$$

and

$$r' = r \cos \zeta \tag{A-2}$$

where F = focal length,

so that the projected surface error would be

$$\Delta z = \frac{r^2}{4F} (1 - \cos^2 \zeta). \tag{A-3}$$

This expression gives the approximate projected surface errors in the radial direction. The surface errors in the angular ζ direction are obviously sinusoidal.

Here the supposed actual surface errors have been accounted for. However, these by no means dictate the exact behavior of phase errors across the radiation

aperture. These surface errors must be weighted with the illumination taper to obtain a phase error function for the aperture. It is also noted that since the periphery of the center section is assumed to be on the true parabolic contour, the actual error in the rib sections near this periphery approaches zero. Thus, a detailed expression for the errors in the rib section would indeed be complex.

The previously described errors might be approximated by a sinusoid whose amplitude is the maximum of the weighted errors previously described. Such a function is compared to the supposed actual errors in Figure A-3. It is noted that this function is less than the supposed actual error; however, this error has already been noted to be larger than the error expected in fabrication.

The supposed actual deviation in Figure A-3 has been weighted by a Gaussian taper, $e^{-2.6r^2}$, where the constant 2.6 was obtained from Reference A-2 for an aperture efficiency of 65 percent, which might be anticipated.

Now considering the mean squared phase error existing across the outer skirt sections, this mean squared phase error, δ_0^2, would be related to the mean squared surface error, $\bar{\Delta}^2$, by

$$\delta_0^2 = (2\beta\bar{\Delta})^2 = \left(\frac{4\pi}{\lambda}\right)^2 \bar{\Delta}^2 \qquad \text{(A-4)}$$

where

β = phase constant in the medium of propagation,

$\beta = 2\pi/\lambda$,

λ = wave length,

$\bar{\Delta}^2$ = mean squared surface error.

if it were assumed that the surface errors may be projected directly to the aperture without modificiation. This approximation improves as f/D decreases.

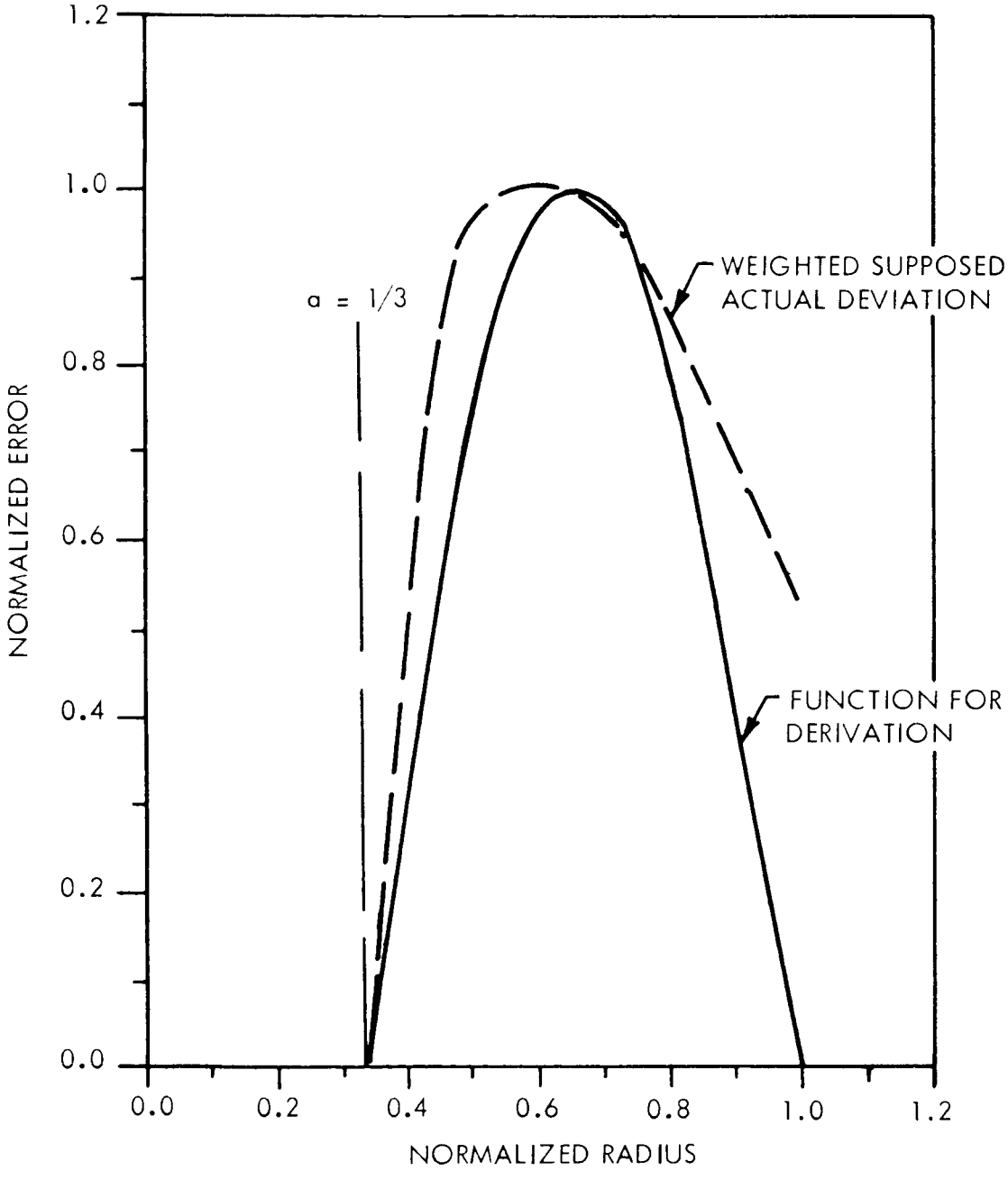

Figure A-3. Comparison of Error Functions in Outer Skirt Sections

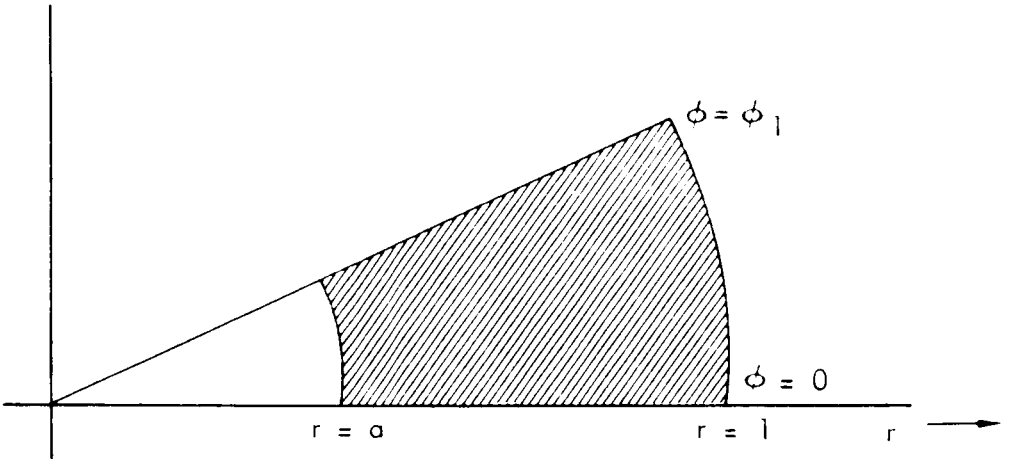

Figure A-4. Geometry for Outer Skirt Error Calculations

The mean squared surface error would be given by

$$\overline{\Delta}^2 = \frac{1}{A} \int_A |\Delta|^2 dA \qquad \text{(A-5)}$$

where

Δ = surface error,

A = area of integration.

In calculating the mean squared phase error over the outer skirt sections, it is noted that this error over the whole surface is the same as the error over one section. Thus, the only area of integration required is a single rib section.

Considering one panel as shown in Figure A-4, the surface error, Δ, as previously reasoned, is expressed by sinusoids in the region of interest.

This surface error function could be expressed as:

$\Delta = 0$ for $0 < r < a$,

$$\Delta = \Delta_m \sin\left(\pi \frac{o}{o_1}\right) \sin \pi \frac{(r-a)}{(1-a)} , \qquad \text{(A-6)}$$

where

Δ_m = maximum weighted deviation,

a = normalized inner radius,

for

$0 \leq o \leq o_1$,

$a \leq r \leq 1$.

Combining Equations A-4, A-5, and A-6, the mean squared phase error may be expressed as

$$\delta_o^2 = \left(\frac{4\pi}{\lambda}\right)^2 \frac{1}{A} \iint \left[\Delta_m \sin\left(\pi \frac{o}{o_1}\right) \sin \pi \frac{(r-a)}{(1-a)}\right]^2 dA, \qquad (A-7)$$

and noting that the area of this region is

$$A = o_1 \, 2, \qquad (A-8)$$

the error would be expressed as

$$\delta_o^2 = \left(\frac{4\pi}{\lambda}\right)^2 \frac{2\Delta_m^2}{o_1} \int_a^1 \int_0^{o_1} \sin^2\left(\pi \frac{o}{o_1}\right) \sin^2\left[\pi \frac{(r-a)}{(1-a)}\right] r \, do \, dr. \qquad (A-9)$$

This expression (Equation A-9), as integrated in Appendix B, gives the mean squared phase error for the outer rib sections as

$$o^2 = \frac{4\pi^2}{\lambda^2} \Delta_m^2 \left[\left(\frac{1-a}{2}\right)^2 \cdot \frac{a}{2} (1-a)\right]. \qquad (A-10)$$

This expression (Equation A-10) gives the mean squared phase error, δ_o^2, for an aperture with errors existing from a radial distance, "a", to 1, whose surface errors are a sine function over this radial distance and whose errors are periodic with the angular displacement o. The maximum surface error is Δ_m.

Rib errors will exist due to manufacturing tolerances etc. These errors are assumed to be distributed in a normal manner. For a rib error, d_R, the projected phase error, δ_R, at the aperture would be

$$\delta_R = 2\beta d_R = 4 \frac{\pi}{\lambda} d_R , \qquad \text{(A-11)}$$

which must now be combined with the phase errors, δ_o, due to the number of rib sections used.

When two functions are independent, the variance of the sum is equal to the sum of their variances. Certainly, the errors in the ribs themselves are quite independent of the choice of number of rib sections. Thus, the total mean squared phase error, δ_T^2, in the outer sections would be given by

$$\delta_T^2 = \delta_o^2 + \delta_R^2 . \qquad \text{(A-12)}$$

The other error to be considered is the error in the center section. Surface errors in this section produce mean squared phase errors, $\bar{\delta}^2$, which will also reduce the aperture efficiency and increase the first side lobe level. The effect of this phase error, $\bar{\delta}$, is considered in the following paragraphs.

3. GAIN REDUCTION

The mean squared phase errors δ_o^2, δ_R^2, and $\bar{\delta}^2$ described in "Surface Error Functions" will contribute to the loss of gain. Since the reduction of aperture efficiency is specified, the reduction of directive gains must be investigated. For an aperture with no blockage, the reduction in directive gain is the reduction in aperture efficiency.

Considering first the gain reduction due to the mean squared phase errors, $\bar{\delta}^2$, in the center section, for correlation intervals much greater than a wave length, Ruze (Reference A-3) has shown this to be

$$\text{gain reduction in center Section} = e^{-\bar{\delta}^2} . \qquad \text{(A-13)}$$

Considering the gain reduction in the outer skirt section, if the errors were random, Equation A-13 could be used. However, a portion of the errors are periodic. Spencer (Reference A-4) has derived an expression for the gain reduction for an aperture with periodic phase errors. This expression is

$$\text{Spencer's gain reduction} = 1 - \delta^2. \tag{A-14}$$

However, this was derived for small phase errors. Observe that this at least limits phase errors to be less than unity. Equation A-13 becomes approximately A-14 when $\bar{\delta}^2$ is much less than 1. Assuming that Equation A-13 more closely describes gain reduction due to any phase errors, the gain reduction in the outer rib section would be given by

$$\text{gain reduction of outer section} = e^{-\delta T^2}. \tag{A-15}$$

Now it becomes necessary to combine the effects of the various phase errors. If the illumination taper used may be approximated as a Gaussian taper, i.e.,

$$F(r) = e^{-pr^2} \tag{A-16}$$

where

F (r) is the normalized voltage across the aperture,

and the aperture efficiency is 65 percent, the corresponding P value is 2.6. For this taper and a normalized inner section radius, a = 1/3, the aperture efficiency of this approximately uniformly illuminated aperture is greater than 99 percent. Using this as unity, the ratio of the gain of the inner aperture to the gain of the total aperture with efficiency, η, would be

$$\frac{G_I}{G_T} = \frac{a^2}{\eta} \tag{A-17}$$

where

G_I = inner aperture gain,

G_T = total aperture gain.

The reduced gain, G'_T, of the reflector due to errors in the skirt section would be

$$G'_T = G_T e^{-\delta T^2}, \tag{A-18}$$

and the gain, G_R, of the outer rib sections alone would be

$$G_R = G'_T - G_I. \tag{A-19}$$

The gain, G, of the aperture would then be

$$G = G'_I + G_R, \tag{A-20}$$

which becomes, after substituting and combining Equations A-13, A-17, A-18, and A-19,

$$G = G_T\left[\frac{a^2}{\eta}\left(e^{-\bar{\delta}^2} - 1\right) + e^{-\delta T^2}\right] \tag{A-21}$$

where

G = reduced gain,
G_T = ideal parabolic gain,
a = normalized radius of inner section,
η = ideal total aperture efficiency,
$\bar{\delta}^2$ = mean squared phase error in inner section,
δ_R^2 = mean squared phase error in ribs,
δ_O^2 = mean squared phase error due to number of rib sections.

This expression was used to show gain reduction for various numbers of rib sections and inner surface tolerances for a 65 percent aperture efficiency and a 9-foot diameter paraboloid shown in Figure 3. The size paraboloid is used in Figure 2 to show gain reduction due to rib errors when the inner surface has no error. The rib 3σ tolerance used is 0.100 inch, which corresponds to an rms tolerance of 0.033 inch.

To investigate the effects of various outside diameters, the errors $\bar{\delta}^2$ and δ_R^2 will be considered to be zero. The maximum weighted surface deviation, Δ_m, is given by Equations A-3 and A-16.

$$\Delta_m = \frac{R_1^2}{4F} (1 - \cos^2 \zeta) e^{-2.6 r_1^2} \tag{A-22}$$

where

Δ_m occurs at radius R_1 or normalized radius, r_1.

For an outside radius, R_o,

$$r_1 = \frac{R_1}{R_o} \tag{A-23}$$

and a constant number of rib sections where ζ is constant, then

$$\Delta_m = K_1 \frac{r_1^2 R_o^2}{F} e^{-2.6 r_1^2}. \tag{A-24}$$

For a fixed f D dish, F/R_o = constant and

$$\Delta_m = K R_o r_1^2 e^{-2.6 r_1^2}. \tag{A-25}$$

Since Δ_m then always occurs at r_1, the maximum weighted surface deviation varies directly with the outside diameter (as might have been seen intuitively).

Using this information, the top graph of Figure A-5 was plotted. This graph is for a 65 percent efficiency with no rib errors or errors in the center section.

In investigating the effects of other aperture efficiencies, only Gaussian tapers will be considered, since most common illumination tapers may be approximated by a Gaussian taper by proper choice of constant. For a constant number of rib sections and fixed diameter, the maximum surface error at radius r_1 is

$$\Delta_m = K_1 r_1 e^{-p r_1^2}. \tag{A-26}$$

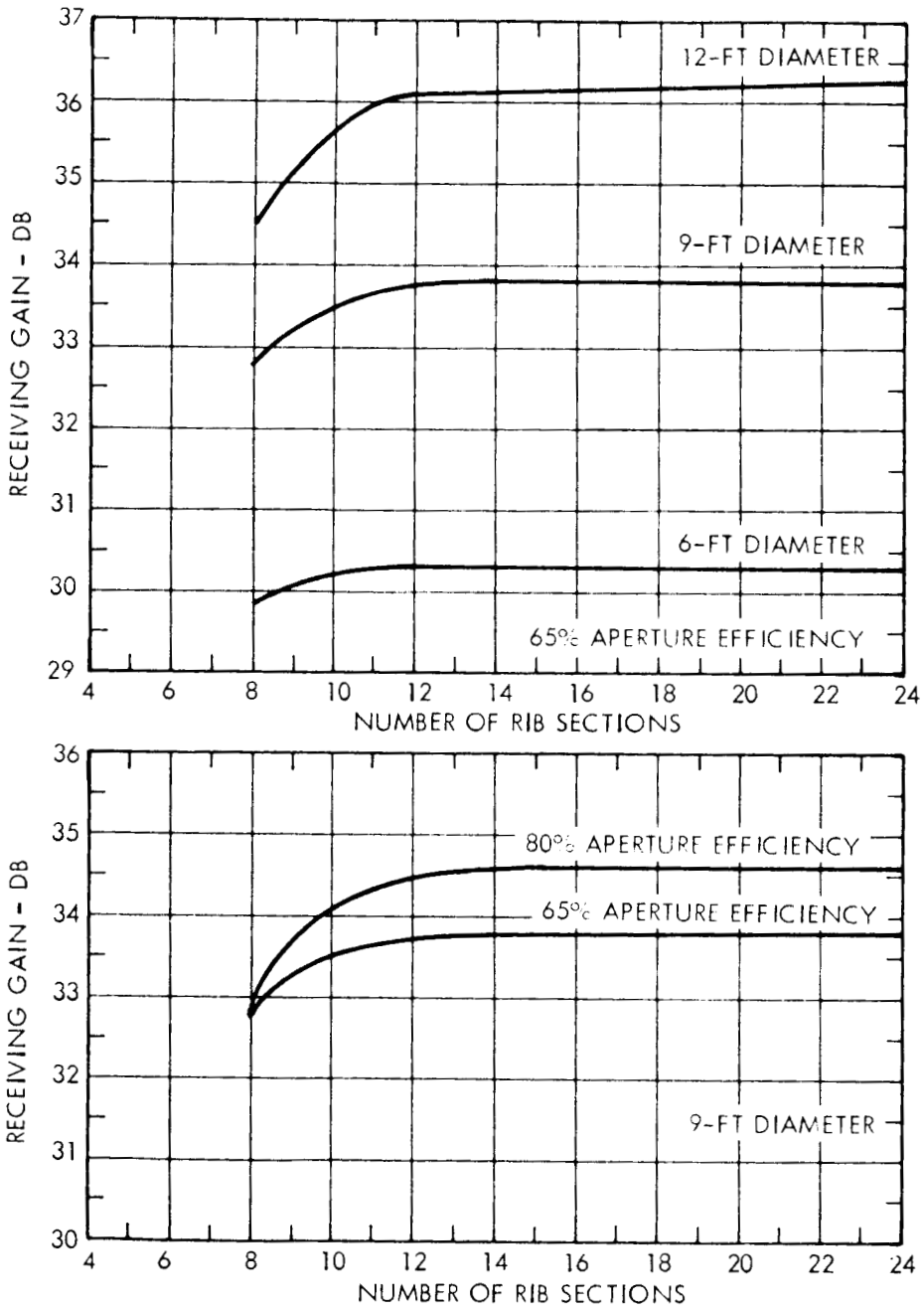

Figure A-5. Gains for Receiving Aperture for Various Numbers of Rib Sections, Aperture Efficiencies, and Diameters when No Errors Exist in the Center Section on Ribs

For p values reasonably close together, the exponential term varies Δ_m much faster than the linear variation with r. From Figure A-3, observing that Δ_m occurs in the vicinity of $r = 0.6$, the behavior of Δ_m with small changes in aperture efficiency could be given by the proportionality,

$$\Delta_m \propto e^{-0.36p} . \qquad \text{(A-27)}$$

For an aperture efficiency of 80 percent, the corresponding p value is 1.6. Using this data, the bottom graph in Figure A-5 was obtained for gain reduction, using two aperture efficiencies.

4. SIDE LOBE PERFORMANCE

Although side lobe performance was not of specific importance, some investigation was made of first side lobe levels that might be expected for various design side lobe levels. Anticipating that the ribs and center section can be built to tolerances such that phase errors from these sources are negligible, the only errors considered here are those in the outer skirt sections.

The only work available on side lobe degradation from errors on a circular aperture is that of Ruze (Reference A-3). Although the work is specifically for random errors, the only difference from the outer skirt errors considered here is that the random errors would tend to be normally distributed about some mean with a particular variance. With the assumed singly curved surface between two ribs, the variance of the mean squared phase error would be zero. Thus, the only difference is that for these well behaved surface errors, it would be 100 percent certain that the side lobe levels would be no higher than predicted. Any inclusion of random errors will degrade this certainty level.

Ruze (Reference A-3) has shown that the resulting side lobe level with phase errors is given by

$$\bar{P}(\theta,\phi) = P_o(\theta,\phi) + S(\theta,\phi)\,4\left(\frac{c}{\lambda}\right)^2 \pi^2 \bar{\delta}^2\, e^{-\left(\frac{\pi C}{\lambda}\sin\theta\right)^2} \quad \text{(A-28)}$$

$$= P_o(\theta,\phi) + P_D(\theta,\phi) \quad \text{(A-29)}$$

where

$P_o(\theta_1\phi)$ = undisturbed power pattern,

$P_D(\theta_1\phi)$ = disturbing pattern,

$\bar{P}(\theta_1\phi)$ = resulting pattern,

$S(\theta_1 o)$ = scattering factor,

C = correlation interval

λ = wave length

θ = angle off main beam axis.

Jasik (Reference A-5, Page 32) gives as the scattering factor for a plane E - M wave, normalized to unity,

$$S(\theta_1\phi) = \frac{(1 + \cos\theta)^2}{4}, \quad \text{(A-30)}$$

which could be used for this aperture.

The correlation interval in Ruze's work (Reference A-3) relates the independence of two errors on the aperture separated by some distance. Examination of the behavior of the correlation interval shows that at a distance of 2C, the errors are approximately 95 percent unrelated. For the 9-foot diameter paraboloid, and C taken to be 3 feet, C/λ is 6.7. Recalling that these surface errors exist only on the outer portions, it appears that the contribution to the side lobe levels, P_D, due to these errors should be reduced, since the outer portions of the aperture have only a part of the total illumination. Examination of the derivation of Equation A-10, however, shows that this is the mean squared phase error over

the entire surface due to weighted surface errors in the outer portions only.

Then for the first side lobe at approximately 5 degrees,

$$P_D = 44.5\bar{\delta}^2. \quad \text{(A-31)}$$

Using $\bar{\delta}^2$ as the $\delta_o{}^2$ in "Gain Reduction", various design side lobe levels should be examined to find the expected first side lobe level for various numbers of outer rib sections. These results are shown in Figure A-6. These results, subject to the approximations made, show the side lobe performance of this paraboloid compared to an ideal paraboloid.

5. TANGENTIAL RIB CONCEPT

A tangential rib concept was studied for larger packaging ratios. When the packaging ratio is defined as the ratio of the opened or unfurled diameter of the paraboloid to the packaged diameter of the unit, the packaging ratio of the rigid rib example discussed so far in this appendix was limited to approximately 3 : 1.

In the tangential rib concept, the rib is wrapped around the periphery of the inner fixed surface while stowed, then allowed to spring into position along a line tangent to that inner fixed surface upon erection. This section reports results of the surface error effects on the gain on the reflector, using the tangential rib concept.

Packaging ratios from 3 : 1 to 8 : 1 are considered for an inside fixed diameter of three feet. The number of ribs varies from 12 to 24. The tolerances used are 0.030 inch rms for the ribs and 0.125 inch rms for the inner fixed surface. The aperture illumination used is a Gaussian taper for a 65 percent illumination efficiency with respect to uniform illumination.

The results were obtained using the work discussed in "Gain Reduction", where

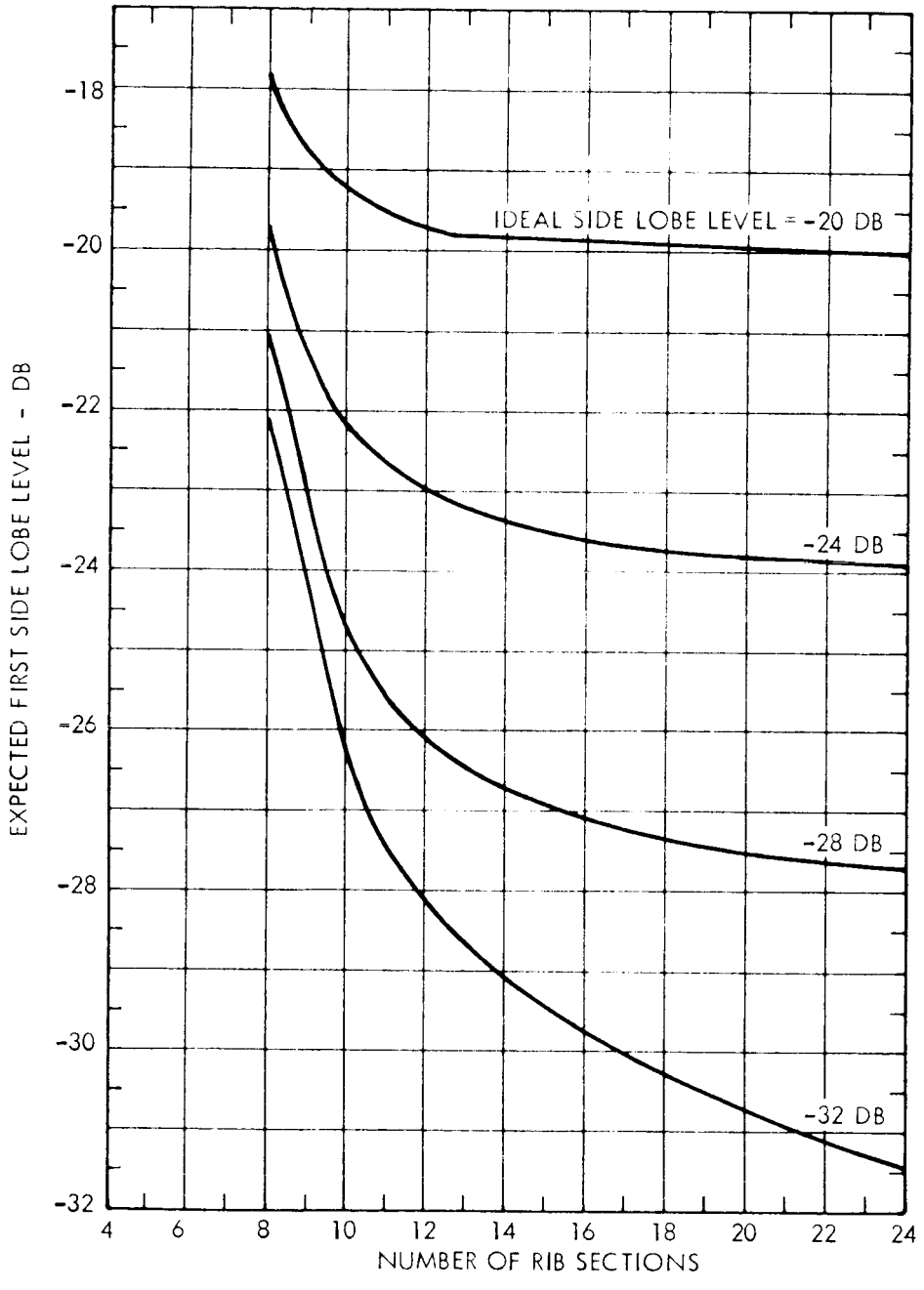

Figure A-6. Expected Side Lobe Levels for Various Numbers of Outer Rib Sections and Ideal Side Lobe Levels (Rib 3σ Tolerance and Inner Surface 3σ Tolerance Less than 0.05 Inch)

the gain reduction, G/G_t, is given by

$$\frac{G}{G_t} = \frac{a^2}{\eta}\left(e^{-\bar{\delta}^2} - 1\right) + e^{-\delta_T^2} \qquad \text{(A-32)}$$

where

η = aperture efficiency,

a = normalized inside radius,

$\bar{\delta}^2$ = mean squared phase error of inner surface,

δ_T^2 = mean squared phase error in rib sections (rib error effects plus effects of nonparabolic surface),

where the mean squared phase error, δ_o^2, of the outer surface due to the ribbed construction is given by

$$\delta_o^2 = \frac{4\pi^2}{\lambda^2}\,\Delta_m^2\left[\left(\frac{1-a}{2}\right)^2 + \frac{a}{2}(1-a)\right] \qquad \text{(A-33)}$$

where

λ = operating wave length,

Δ_m = maximum weighted surface deviation,

a = normalized inside radius.

The results of this supplementing study are shown graphically in Figure 4. The gain reduction (or more specifically, loss of directivity) is shown as a function of outside diameter and number of rib sections.

APPENDIX B. INTEGRATION OF OUTER SECTION MEAN SQUARED PHASE ERROR EXPRESSION

The mean squared phase error for the outer rib sections is expressed in Equation A-9 of Appendix A. The equation contains the integral

$$\int_a^1 \int_0^{\phi_1} r \sin^2\left(\pi \frac{\phi}{\phi_1}\right) \sin^2\left[\pi \frac{(r-a)}{(1-a)}\right] d\phi dr,$$

which could be handled first by letting

$$\pi \frac{\phi}{\phi_1} = \theta \text{ and } d\phi = \frac{\phi_1}{\pi} d\theta,$$

so that the integral becomes

$$\frac{\phi_1}{2} \int_a^2 r \sin^2\left[\pi \frac{(r-a)}{(1-a)}\right] d\theta dr,$$

where the integration in θ may be carried out. Upon substituting limits, the integral becomes

$$\frac{\phi_1}{2} \int_a^1 r \sin^2\left[\pi \frac{(r-a)}{(1-a)}\right] dr.$$

Now letting $r - a = x$, $dr = dx$, and $r = x + a$,

$$\frac{\phi_1}{2}\left[\int_0^{1-a} x \sin^2\left(\frac{\pi x}{1-a}\right) dx + a \int_0^{1-a} \sin^2\left(\frac{\pi x}{1-a}\right) dx\right].$$

Letting $\frac{\pi x}{1-a} = y$ and $dx = \frac{1-a}{\pi} dy$,

$$\frac{\phi_1}{2}\left[\frac{(1-a)^2}{\pi^2}\int_0^{\pi} y \sin^2 y dy + \frac{a}{\pi}(1-a)\int_0^{\pi} \sin^2 y dy\right],$$

where the integration yields

$$\frac{\phi_1}{2}\left\{\left(\frac{1-a}{\pi}\right)^2\left[\frac{y^2}{4} - \frac{y}{4}\sin 2y - 1/8 \cos 2y\right]_0^{\pi}\right.$$

$$\left. + \frac{a}{\pi}(1-a)\left[-1/2 \cos y \sin y + \frac{y}{2}\right]_0^{\pi}\right\}.$$

Now upon applying limits and combining terms, this integral is expressed as

$$\int_a^1 \int_0^{\phi_1} r \sin^2\left(\pi \frac{\varphi}{\phi_1}\right) \sin^2\left[\pi \frac{(r-a)}{(1-a)}\right] d\phi dr =$$

$$\frac{\phi_1}{2}\left[\left(\frac{1-a}{2}\right)^2 + \frac{a}{2}(1-a)\right].$$

APPENDIX C. REFERENCES

1. Metals Handbook, Volume 1, Eighth Edition, American Society for Metals.

2. MIL-HNBK-5, August 1962 Edition.

3. Structures Design Manual, Goodyear Aerospace Corporation, Akron, Ohio, April 1962.

4. High-Gain Spacecraft Antenna, GAP-1588, Goodyear Aerospace Corporation, Akron, Ohio, 20 July 1962.

A-1. High-Gain Spacecraft Antenna, GAP-1588, Goodyear Aerospace Corporation, Akron, Ohio, 20 July 1962.

A-2. Doundoulis, P., and Gethin, S., "Far-Field Pattern of Circular Paraboloidal Reflectors," IRE National Convention Record, Part I, March 1959, p 155.

A-3. Ruze, John, Physical Limitations on Antennas, MIT Tech. Report 248, 30 October 1952, p 38.

A-4. Spencer, R. C., A Least Square Analysis of the Effect of Phase Errors on Antenna Gain, AFCRC Report 5025, January 1949.

A-5. Jasik, Henry, Antenna Engineering Handbook, McGraw-Hill, 1961, p 2 - 9.